catalysts

MDPI

Review

Recent Breakthrough in Layered Double Hydroxides and Their Applications in Petroleum, Green Energy, and Environmental Remediation

Mohsen S. Mostafa [1,2,*], Lan Chen [1,*], Mohamed S. Selim [3,4], Ruiyi Zhang [1] and Guanglu Ge [1]

[1] CAS Key Laboratory of Standardization and Measurement for Nanotechnology, CAS Center for Excellence in Nanoscience, National Center for Nanoscience and Technology, Beijing 100190, China; zhangry2018@nanoctr.cn (R.Z.); gegel@nanoctr.cn (G.G.)
[2] Refining Department, Egyptian Petroleum Research Institute, Nasr City, Cairo 11727, Egypt
[3] Petroleum Application Department, Egyptian Petroleum Research Institute, Nasr City, Cairo 11727, Egypt; mohamedselim@gdut.edu.cn
[4] School of Chemical Engineering and Light Industry, Guangdong University of Technology, Guangzhou 510006, China
* Correspondence: mohamed2018@nanoctr.cn (M.S.M.); chenlan@nanoctr.cn (L.C.)

Abstract: The fast development of the world civilization is continuously based on huge energy consumption. The extra-consumption of fossil fuel (petroleum, coal, and gas) in past decades has caused several political and environmental crises. Accordingly, the world, and especially the scientific community, should discover alternative energy sources to safe-guard our future from severe climate changes. Hydrogen is the ideal energy carrier, where nanomaterials, like layered double hydroxides (LDHs), play a great role in hydrogen production from clean/renewable sources. Here, we review the applications of LDHs in petroleum for the first time, as well as the recent breakthrough in the synthesis of 1D-LDHs and their applications in water splitting to H_2. By 1D-LDHs, it is possible to overcome the drawbacks of commercial TiO_2, such as its wide bandgap energy (3.2 eV) and working only in the UV-region. Now, we can use TiO_2-modified structures for infrared (IR)-induced water splitting to hydrogen. Extending the performance of TiO_2 into the IR-region, which includes 53% of sunlight by 1D-LDHs, guarantees high hydrogen evolution rates during the day and night and in cloudy conditions. This is a breakthrough for global hydrogen production and environmental remediation.

Keywords: hydrogen; layered double hydroxides; water splitting; bandgap energy; environmental remediation

Citation: Mostafa, M.S.; Chen, L.; Selim, M.S.; Zhang, R.; Ge, G. Recent Breakthrough in Layered Double Hydroxides and Their Applications in Petroleum, Green Energy, and Environmental Remediation. *Catalysts* **2022**, *12*, 792. https://doi.org/10.3390/catal12070792

Academic Editor: Maria A. Goula

Received: 22 June 2022
Accepted: 18 July 2022
Published: 19 July 2022

1. Introduction

Nowadays, huge amounts of energy have been consumed to make the world civilization flourishing and continuous. Petroleum (crude oil) was the main source of energy for more than one century [1], and it is considered that it will play this role for further decades. Crude oil is a naturally occurring source of energy that consists mainly of hydrocarbons (from C_5 to C_{40+}, Figure 1) with minor portions of S, O_2, and N_2 compounds [2,3].

Raw crude oil is not suitable for direct use as an energy source or in internal combustion engines and must be purified by many physical and chemical treatments. The physical treatment involves washing, sweetening, and then atmospheric/vacuum distillation. Distillations of crude oil result in its fractionation into light cuts (C_5 gases, naphtha, or gasoline), middle cuts (kerosene/jet fuel and diesel), and heavy cuts (heavy gas oil, lubricant oil, wax, and bitumen/asphalt). The primary distilled portions usually contain undesired metals and S, O_2, and N_2 contaminants, which can cause dangerous destruction in refining, storage, and combustion equipment [4]. Hence, chemical treatments, such as hydrodesulphurization, hydroisomerization, hydrodemetalization, and hydrocracking, are required to remove such contaminants and upgrade the petroleum fraction for saving

usage to a certain extent. The chemical treatment in the petroleum industry is known as hydro-finishing. However, the combustion of gasoline, kerosene, and diesel produces SO_x and NO_x by the remaining S and N_2 impurities (10–500 ppm) and can cause acid rains and ozone-depletion [4]. This has a negative impact on the environment as a whole and on plants, animals, and human health.

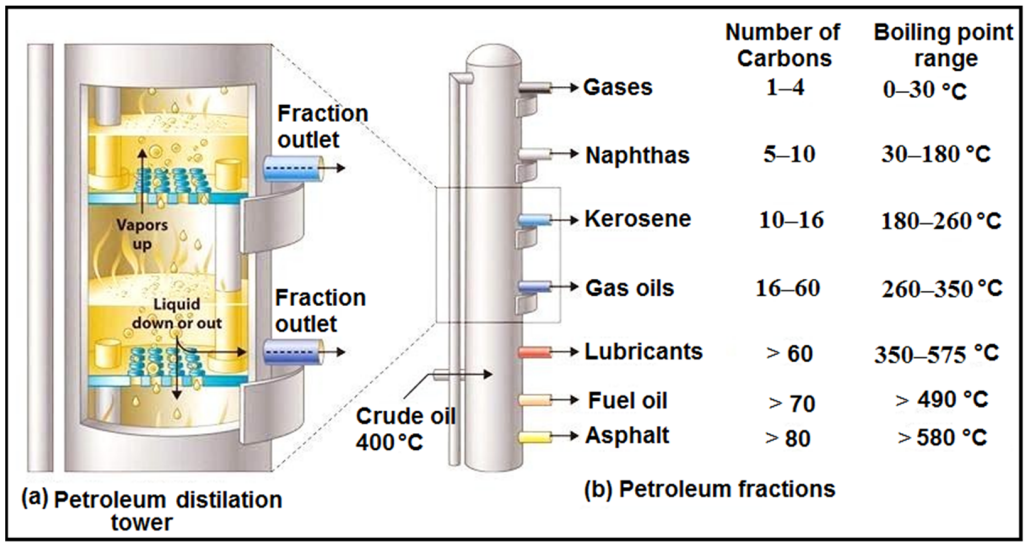

Figure 1. Boiling point distribution and chemical distribution of crude oil components.

In recent years, many parts of the world suffered from different crises due to the current climate states. Germany in Europe faced unexpected floods; North America suffered from exceptional heatwaves; Spain, Turkey, Tunisia, and California recorded dangerous wildfires; and there were abnormally cold conditions in Mexico, while extreme rainfall and precipitation were recorded in Henan province (China). These climate accidents were announced by the world meteorological organization's (WMO) report (Geneva, 31 October 2021). Additionally, the temperature rising caused ocean warming and acidification, elevation in sea-levels, and increasing greenhouse gas concentrations (CH_4 = 1889 ppm, N_2O = 333.2 ppm, and CO_2 = 413.2 ppm). This difference in the earth's near-surface air temperature critically affects global food security. It became a fact that the consumption of coal and petroleum as main sources of energy causes ozone-depletion and climate change [5,6]. The WMO clearly stated that alternative solutions should be found to safe-guard millions of people, coastal cities, and the ecosystem from this negative climate warming. The suggested solution, according to the WMO, to safeguard our future is to build world cooperation for encouraging the dependence on hydrogen within the framework of COP26.

Hydrogen is the ideal fuel to substitute petroleum or at least reduce its extra-consumption. Firstly, hydrogen has a high caloric value, and secondly, it can be produced, transported, and burnt in clean and green tracks [4]. Although the world still depends on petroleum and fossil fuels, the world's hydrogen production is by steam-reforming of hydrocarbons, and only about 5% of hydrogen can be obtained through water electrolysis [7], and the hydrogen produced by photocatalytic water splitting can almost be ignored.

2. Photocatalytic Water Splitting to Hydrogen

Water splitting is an endothermic chemical process that involves the dissociation of water into its main constituents: oxygen and hydrogen. In contrast to conventional electrolysis, which depends on an external direct current to cause water dissociation, water splitting depends on using certain catalytic materials to undertake the O-H bond cleavage. The first photocatalytic water splitting process was practically performed by Fujishima and Honda in 1972 by using a photoelectrochemical cell and TiO_2 as photocatalyst [8]. The photocatalytic water splitting process occurs on the photocatalyst (semiconductor)

surface, according to the following mechanism, where the semiconductor should own a suitable bandgap to harvest and react with certain light photons (of a specific wavelength). Here, the light-photons cause excitation of the electrons in the valence band (VB) of the semiconductor, and when the electrons gain sufficient energy from photons, they migrate to the higher atomic level in the conduction band (CB). The migration of the excited electrons creates excited holes (h^+) in the VB, where water molecules can be effectively oxidized into –OH/O_2 and protons (H^+). The created protons by water splitting in the VB are then reduced into hydrogen by the excited electrons (e^-) in the CB. The oxidation/reduction of water in the VB/CB occurs only if there is no fast recombination between the excited electrons and holes [9].

There are two types of the photo-induced water splitting: (1) photochemical water splitting, in which only a suitable photocatalyst is used to harvest the light photons and split water; (2) the photo-electrochemical method, where external electrical energy (current) is applied to motivate the water splitting by the light/photocatalyst [10]. It is obvious that photochemical water splitting is the potential route for convenient hydrogen production from renewable sources (sun and water) in a feasible/economic pathway. This, in turn, reflects the vital role of photocatalytic materials (semiconductors) and how they can guarantee renewable and clean energy for the world, instead of fossil fuels.

3. General Introduction of Semiconductors

Generally, a semiconducting material has intermediate electron mobility (conductivity), and it is not conductive in normal conditions but can be conductive after certain modifications. Semiconductors have sufficient electrons in the valence band and conduction band and a gap between these two bands. This gap restricts the electron mobility (electrical current) in normal conditions, but the mobility can be improved by simple treatment [11]. In photocatalysis, electron mobility occurs in semiconductors by the excitation of light.

3.1. Commonly Used Semiconductors for Photocatalysis

3.1.1. TiO_2

TiO_2 is the most common and first applied semiconductor in photocatalysis [12], as it is naturally abundant, environmentally friendly, and chemically stable, and it can be synthesized by versatile preparation routes in various morphologies [1,5]. However, photocatalysis by pure TiO_2 is rare, which restricts its work in the UV-region to including only 5% of sunlight radiation [1,5] due to its wide bandgap (3.2 eV) and the fast recombination of the electrons/hole pairs [1,5]. To overcome these drawbacks, many efforts have been made to prepare modified TiO_2 structures, such as Pt-modified TiO_2 [13], Au-modified TiO_2 [14], Ag-modified TiO_2 [15], perovskite (CaTi, SrTi, BaTi)-modified TiO_2 [16], Carbon-modified TiO_2 [17], metal (Co, Ni, Zn)-modified TiO_2 [18], TiN-composites [19], graphine/TiO_2 nanoparticles [20], titania/hydroxyapatite (TiO2/HAp) composites [21], and silica modified titania (TiO_2-SiO_2) [22], etc.

3.1.2. ZnO

The zinc oxide photocatalyst is another N-type semiconductor with a close wide band gap energy to that of TiO_2 (3.37 eV), and it can also be produced by potential methods, such as flame spray pyrolysis, thermal decomposition, and hydrothermal synthesis. ZnO finds wide applications in the UV-region for photodegradation of organic pollutants [19,23], water splitting, and various photosynthesis applications.

3.1.3. CdS

Recently, CdS has drawn much attention as a predominant photocatalyst in various fields of energy conversion/production and environmental remediation. CdS has a great advantage over TiO_2 due to its own narrower bandgap (2.4 eV) and excellent activity in the visible light region, which counts for about 50% of the solar light [20,24]. Accordingly,

recent and numerous studies have reported the applications of CdS in water splitting (for both H_2 and O_2 evolution) and photodegradation of environmental hazards.

3.1.4. CuS

The bandgap energy of CuS can vary from 1.8 to ~2.2 eV and can be prepared by various methodologies [21,25]. These features promote the use of CdS in diverse fields of photocatalysis in a pure form or in combined phases with other semiconductors.

3.1.5. BiO_x

Bismuth oxides (BiO_x) are highly active n-type semiconductors, and there is worldwide attention now for employing advanced BiO_x-nanostructures for green energy production and environmental remediation [1]. The high photocatalytic activities of BiO_x have allowed their applications with other semiconductors, such as CoO_x and TiO_2, for enhanced water splitting to O_2 and/or H_2 [1,5].

3.1.6. MnO_2

The Manganese element has variable oxidation states and provides various oxide forms. The alpha-form (α-MnO_2) is the common form in photocatalysis, and it has the advantage over many catalysts due to its capability to work effectively, even at very low temperatures. Due to the efficient lattice vacancies and oxygen defects both acting as charge carriers, MnO_2 finds wide applications in photocatalysis and especially in photodegradation of organic pollutants [26].

4. The Contribution of Nanomaterials in Energy and Environmental Remediation

Parallel to the discovery of petroleum, various types of materials were also discovered and applied in crude oil production, consumption, and treatment to reduce or eliminate the associated environmental pollution. Firstly, bulky materials containing common elements, such as aluminum [27] and silicon [28], and naturally occurring materials, such as clays and zeolites, were used [29,30]. Since 1998, a new era of nanotechnology and nanomaterials has flourished. Nanotechnology is the science and technology of the preparation, characterization, and application of nanomaterials, i.e., the materials of a crystal size ranging from 1 to <100 nanometers [31]. Nanomaterials have better and different properties than bulky materials due to the restricted electronic motion in the new nano-sized environment. The discovered nanomaterials involve carbon nanotubes (CNTs) [32] graphene sheets [33], metal-organic frameworks [34,35], polymer nanocomposites [36], quantum dots [37], single crystals [38], core shells [39], and layered double hydroxides (LDHs).

Compared to the other nanomaterials that have been explored to date, LDH-based materials have acquired worldwide attention by their unique two-dimensional (2D) and well-tunable structures, in addition to their remarkable optical/electrochemical properties [40–44]. LDHs own high adsorption capacities and tunable bandgaps, and they can effectively supply separated reduction and oxidation reaction corners for green energy production instead of fossil fuels, as in the case of H_2 and O_2 evolution reactions [45–48]. The lamellar structure of LDH-structures allows the formation of variable crystal sizes, shapes, and morphologies parallel to different types of interlayer cations and anions. In the field of green energy production, these features effectively improve the efficiency of charge transfer/separation and, in-turn, the net reactivates (photo-activities) of the catalysts (photocatalysts) derived from LDHs and the energy production process as a whole [47,49–51]. Based on the recent global interest in LDHs, numerous studies and review articles have been published to estimate the beneficial properties and role of LDHs in energy and/or environmental applications. A review by Fan et al. [52] discussed the preparation routes of some LDH-structures and their related catalytic applications, while Mohapatra et al. [46] extensively studied progress in the LDH-fabrication and photocatalytic applications in pollution control, H_2-evolution, and CO_2-reduction to valuable chemical intermediates; the author could state 164 references in these fields in 2016. The complexities of LDH-

applications in the environmental remediation through the removal of dyes were also reviewed by Yang [53]. Again, a mini-review was published by Yan [47] focusing on discussing the advances in LDH-synthesizing for H_2/O_2-enhancement. The relationship between structure and activity and its effect on photochemical/electrochemical water splitting and CO_2-reduction was reviewed by Zhao et al. [11]. Wu et al. [54] discussed progress in constructing heterostructures from LDH, with respect to both synthesis methods and structural growth. Recently, in 2020, a review by Yang et al. [55] discussed the tailoring and engineering of LDHs/modified LDHs catalysts for feasible water treatment. Parallel to Yang et al., Razzaqet al. [56] published a study concerning the application of some LDH-semiconductors in CO_2 conversion, and the authors also mentioned the advancement in synthesis routes of both LDHs and LDH-derived materials, as well as the reaction conditions affecting their catalytic activities [57]. Applications of LDH-nanocomposites in artificial photosynthesis and the role of the synthesis and modification conditions in this process were summarized recently in 2021 [58]. The effect of the synthesis and modification of LDH photoactive materials in photo-electrocatalysts was reviewed and published by many investigators [40,58].

By following the publications of LDHs, it seems that the field of LDH-based photocatalysis is very crowded, but there is almost no work reviewing the recent bandgap tailoring of LDH-nanomaterials and their application in petroleum, according to our knowledge. We are going to mention the recent progress made in LDH-bandgap engineering, as well as their applications in the petroleum field and treatment of the related hazards that emerged from the combustion of fossil fuel. Thus, this review will focus on LDH-modulation and how to make use of their excellent physical/chemical properties to enhance the recent green energy route and enhance the environmental remediation through the effective removal of petroleum-based hazards and water treatment. The review will highlight the role of LDHs/LDH-derived materials with respect to the removal of air pollution, sulfur, and organic contaminants. A futuristic trend discussing the conversion of 2D LDHs to 1D LDHs through modified synthetic techniques and the impact of these novel 1D LDHs in improving the water/green energy routes will be highlighted.

5. General Introduction of Layered Double Hydroxides (LDHs)

LDHs are well-known 2D layered materials and are sometimes nominated as hydrotalcites or anionic clay minerals due to their abilities to intercalate with negative ions in contrast to cationic clay minerals as naturally occurring clay and zeolites. The chemical structure and nature of LDHs can be well-understood by recalling the structure of the parental and naturally occurring brucite. Brucite is an octahedral form of magnesium hydroxide [$Mg(OH)_2$], in which the Mg^{2+} ions coordinate in an octahedral six-fold to OH-shared edges, forming infinite symmetrical and repeatable sheets or layers. These sheets are stacked on top of each other and are bonded together by hydrogen bonds, as shown in Figure 2 [59,60].

The structure of LDHs is originated when some divalent ions, such as Mg^{2+} ions, are substituted by trivalent ions with a comparable radius, and this substitution yields a positive charge through the hydroxyl sheet (brucite-layer). The net positive charges are compensated by negative ions to neutralize the final structure of any LDH [27]. The negative ions usually lie in the interlayer region between the two brucite-sheets. The negative ions are indicated as interlayer ions. Besides the interlayer ions, and between the interlayer spaces, water molecules are permanently present as intercalated water. This water is so-called interlayer water or crystal water; hence, the main LDH structure is built and determined by the nature of the brucite-like sheets, the position of anions and water in the interlayer region, and the type of stacking of the brucite-like sheets. The sheets containing cations are built as in brucite, where the cations randomly occupy the octahedral holes in the close-packed configuration of the OH ions.

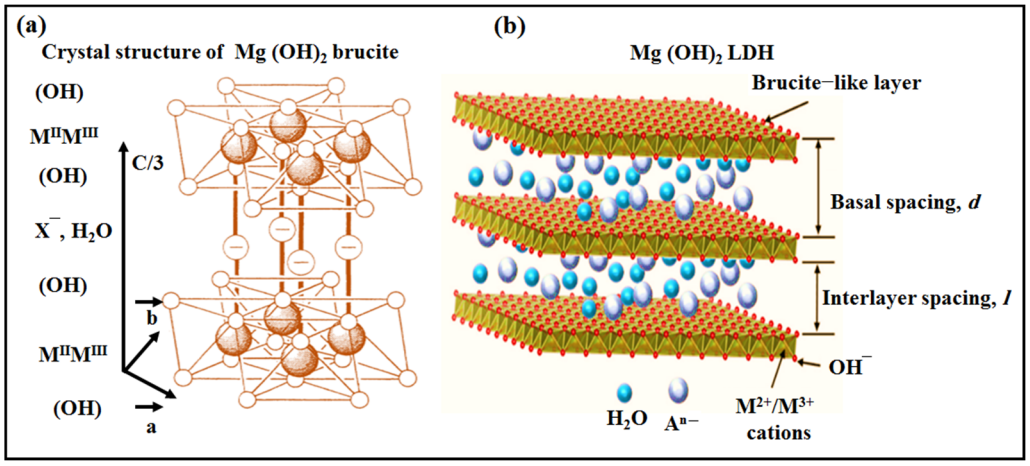

Figure 2. Structures of (**a**) Mg $(OH)_2$ brucite (Adopted from Cavani et al. [59], with permission from Elsevier) and (**b**) LDH (Reprinted with permission from Ref. [60]. Copyright 2020, MDPI).

5.1. General Formula of LDHs

The general formula can be written as $[M_{2+1-x}M_{3+x}\ (OH)_2]_{x+}[An_{-}x/n.yH_2O]_{x-}$, where M^{2+} is a divalent metal ion, M^{3+} is a trivalent metal ion, An- is an interlayer exchangeable anion, y is the count of water molecules, and x is the coefficient factor resembling the molar percentage between M^{2+} to M^{3+}, where LDH structures can exist for the value of x in the range 0.1 to 0.5; many indications show that it is possible to obtain pure LDHs only in the range of 0.2 to 0.33 [6,61].

5.2. General Characteristics of LDHs

5.2.1. Memory Effect

It is a characteristic feature of LDHs that the primary structure of LDHs can be retained and recovered again after calcination at elevated temperatures by subjecting the oxide form into water containing different anions. The memory effect property of LDHs is used to introduce and substitute different anions into the LDH gallery, giving rise to versatile structures and different compositions of LDHs for drug delivery and DNA storage.

5.2.2. High Surface Area

LDHs have great surface areas due to their low dimension, infinite lamellar (layered) structure, and very small particle sizes. According to the IUPAC classification, LDHs usually exhibits IV-type isotherms, with H3 hysteresis loop characteristics for the mesoporous materials [1,6]. Although LDHs exhibit usual IV-type isotherms, the values of their surface area are variable. Table 1 shows the variation of the surface area of LDHs with their type and synthesis route.

5.2.3. Intercalation Reactions

Intercalation reactions of LDHs are known also as host–guest reactions, which involve the substitution of the main interlayer anion (the anion linking the LDH-layers) with another anion or molecule. The intercalation reactions in LDHs can be performed by the memory effect as above-mentioned or by an ion-exchange mechanism, which involves immersion of the freshly prepared LDH in a highly concentrated solution of the guest anion to be intercalated.

5.2.4. Layer-by-Layer (LbL) Assembly

Layer-by-layer assembly involves electrostatic interactions between guest species and a parental LDH-host and relies on alternative dipping of a substrate into a suspension of positively charged LDH-nanosheets and a solution of negatively charged guest anions. This technique can involve co-assembly through a poly-anion carrier, when positively

charged ions or neutral molecules act as guest species. Preferred nanohybrids can be achieved when the positively charged LDH-nanosheets and negatively charged guest anions coexist in an aqueous medium to facilitate exfoliation assembly towards a core-shell or porous structures. Additionally, the LBL-assembly can provide a great route toward solid devices with multifunctionality and ultrathin films (UTFs) with anisotropic properties and a preferred orientation when applying an external field (magnetic or electric field) during high guest loading into the parental LDH [62].

Acid–Base Properties

Different elements of variable oxidation statistics can be applied in the preparation of LDHs, according to the nature of the primary physical properties of the starting element; the final LDH has its own acidic, basic, or acidic–basic property.

Formation of Thermally Stable Mixed Oxides

LDHs are two-dimensional isotactic materials with sharp crystalline structures that originated from homogeneous intercalation and the substitution of different metals. Accordingly, the mixed oxides produced from the calcination of LDHs have very stable thermal structures due to the infinite solid state chemical interactions that occurred through the thermal treatment.

5.2.5. Synthesis Methods for LDHs

There are several methods to prepare LDHs, and each method has its own effect on the surface morphology and physical and chemical properties of the produced LDHs.

Co-Precipitation Method

This is the most common method applied for the preparation of LDHs [63–65] and nanomaterials generally, in which the metal cations are mixed in a dilute solution under vigorous stirring at 50–90 °C. On the other hand, the precipitation of the metal cations is performed through a suitable base titration in the presence of a carbonate source. The common bases applied for precipitation are NaOH and NH_4OH, and the carbonate species are applied in general by Na_2CO_3. Carbonate is the most stable and common interlayer anion, so it is extremely difficult to prepare LDH material free of carbonate without severe precautions. The factors leading to the formation of LDH, rather than amorphous hydroxide or gel formation are aging time, rate of titration, and pH. A long aging time (12–36 h) and slow rate of titration improve the crystallinity and the general morphology of the produced LDH, while pH must be adjusted between 9 and 12. The range of pH is wide ($\geq$8), whereby it must be above the neutralization point (pH = 7) to ensure full precipitation of the cations (since LDH is a true hydroxide). High pH values can affect the morphology and crystallinity of LDHs [66], as they increases the cationic content (M^{II}–M^{III}) in the final LDH [67].

A long aging time ($\geq$12 h) increases the crystallinity as well as the cationic content of the formed LDH [67]. High temperatures accelerate the full precipitation of LDHs and increase their crystallinities [68].

Hydrothermal Method

It is similar to the co-precipitation method, but the process is completed under the vapor pressure produced from the entrapped solution of the metal cations and precipitating agents in a Teflon-lined autoclave at an elevated temperature (120–180 °C) for a long time. The hydrothermal method can be performed by firstly precipitating the starting cations, as in the precipitation method, and then transporting the precipitate into the autoclave, or it can be completely performed in the autoclave [69,70]. Due to the high temperature and long-time of synthesis, the hydrothermal method usually yields LDHs that are sharply crystalline, of a high surface area, porous, and, in-turn, highly active adsorbents/catalysts.

Sol-Gel Method

This is that in which the precursors of the metals to be precipitated are in the form of alkoxides, such as aluminum tri-isoperoxide and titanium tetra-isoperoxide, rather than the conventional inorganic anions, such as chlorides or nitrates. The precipitation procedure can be completed by the self-hydrolysis of the used alkoxides by heating up to 70 °C for a definite time or by applying a suitable hydroxide to control the final pH [71,72].

Vapor Diffusion Method to Prepare Exceptional Ti-Containing LDHs

The recently modified method to prepare highly crystalline and ultra-thin Ti-containing LDHs was introduced in 2020 by Mostafa et al. [73]. Common Ti-based LDHs exhibit low crystallinities due to the segregation of Ti during the preparation by conventional precipitation methods [74–76]. For the first time, we applied the diffusion of the $TiCl_4$ vapor method to avoid such segregation and could synthesize novel CoTi-LDH nanorods of exceptional photocatalytic properties. The used Cl^--precursors led to 1D-assembly by longitudinal propagation of $CoCl_2$ and $TiCl_4$ precursors and the formation of a $[TiCl_6]^{2-}$ intermediate during the nucleation stages of the LDH structure. This, in turn, greatly enhanced the chemical activity by the ultrathin assembly of CoTi-LDH by the presence of most of the atoms on the surface of the nanorods [77] in contrast to the conventional 2D structure of common LDHs. As a result, the prepared 1D CoTi-LDH exhibits a lowered bandgap energy and great IR-responsivity (1.4 eV), high oxidation states of both Co and Ti, and excellent catalyst distribution in the water splitting media. This innovative vapor diffusion method can be industrially commercialized, especially for massive production of Ti-containing LDHs for prospective water splitting, solar cells' materials, and other catalytic and photocatalytic applications. The nature liquid state of $TiCl_4$ facilitates the usage of the vapor diffusion method by the self-supplied $TiCl_4$–vapor or by the use of an inert carrier, such as N_2, without the need for a dosing pump, such as in continuous flow preparation methods.

Continuous Flow Preparation Method

Because LDHs are highly active and promising materials in fields of energy and the environment, the development of innovative methods for the scaled-up preparation of LDHs is necessary. The abovementioned preparation methods of LDHs are common, feasible, and long-term trialed since the discovery of LDHs, but they still suffer some drawbacks, which hinder the industrial production of LDHs. The recent continuous flow preparation methods achieve great advantages over conventional methods (batch precipitation) in the preparation of LDHs, such as the feasible scaling up and better physical/chemical properties of the manufactured materials [78]. The synthesized LDHs by flow routes exhibit narrower particle sizes, much finer morphologies, and high surface areas. By the flow chemistry routes, it is now possible now to avoid the drawbacks of batch methods, such as an unstable pH, the super-saturation stage, agglomeration, and time consumption, especially in the conventional co-precipitation methods [79]. The continuous flow preparation methods have various reactor designs, as well as diverse operation means and configurations for the preparation of LDHs and other materials in specific morphologies and compositions [79]. The great benefits of the flow chemistry technique make it the promising route for supplying the research and industrial communities with smart and tailored LDH and other valuable materials.

Table 1. Correlation between the chemical composition and synthesis route of LDHs and surface area [80–88].

LDH	M^{II}/M^{III} Ratio	Synthesis Route	Specific Surface Area (m^2/g)	Ref.
$CoAlCl^-$	4:1	Hydrothermal/acid salt template	26.5	[80]
$CoAlCl^-$	4:1	Coprecipitation	30.9	[80]
$CoAlCl^-$	4:1	Hydrothermal	19.7	[80]
$NiAlCO_3^{2-}$	1:1	Coprecipitation	133	[81]
$NiCoNO_3^-$	1:1	Hydrothermal	37	[82]
$NiFeCO_3^-$	2:1	Coprecipitation	427.00	[83]
$NiAlCl^-$	4:1	Coprecipitation	95.44	[84]
$NiAlCO_3^-$	4:1	Hydrothermal	13	[84]
$MgFeCl^-$	2:1	Solvothermal with SDS	70.19	[85]
$ZnAlCl^-$	2:1	Urea	253	[86]
$ZnMgAlCO_3^{2-}$	2:1	Coprecipitation	28.12	[87]
$NiFeNO_3^-$	4:1	Coprecipitation	17.84	[88]

5.2.6. Characteristic Analyses of LDHs

LDHs have their own characteristic structures and morphologies, besides their general characteristics as the other nanomaterials. There are two main instrumental analyses that can be used to analyze the preparation of LDH.

X-ray Diffraction (XRD)

The XRD diffraction patterns of LDHs are fingerprints and merely offer evidence for the formation of the LDH structure, rather than the ordinary hydroxide or any bulk or nanostructured material. LDHs usually show the hydrotalcite structure [1,6] as the only structure existing through the sample, according to the JCPDS file no. 22-700, characterized by sharp, narrow, and symmetric reflections respective to the low 2 theta of basal (003), (006), and (009) planes, in addition to asymmetric and broad reflections at the higher 2 theta for non-basal (012), (015), and (018) planes. These successive diffractions by basal planes d (003) = 2d (006) = 3d (009) of LDH refer to fully packed stacks of brucite-like layers ordered along the c-axis, which represent the thickness of the brucite layer and the interlayer distance. The XRD patterns of LDHs are unique and mostly the same, and whatever the metals applied in the LDH preparation and construction, a difference may be noticed only in the d-spacing between the successive planes; Figure 3 shows a typical XRD of M^IM^{III} LDH.

Surface Features of LDHs; Scanning Electron Microscopy (SEM), High Resolution Transmission Electron Microscope (HRTEM), and Surface Area

SEM is the second analytical tool that reflects the hydrotalcite structure of LDHs. The SEM images of LDHs usually reveal plate-like morphologies with well-ordered hexagonal crystallites [6] of a high porosity, as shown in Figure 4. In contrast to SEM and XRD, which are characteristic analytical tools for LDH and provide a fingerprint image of the LDH-structure, HRTEM imaging of LDHs is variable, where sometimes it clearly reflects the 2D assembly of the hexagonal plate crystallites of LDHs (as SEM) [63], but in other times, it provides unclear or confusing images due to the finite LDH structure and the new electro/electromagnetic properties of elements in the LDH configuration [64]. Figure 5A,B shows variable HRTE-images of common LDHs.

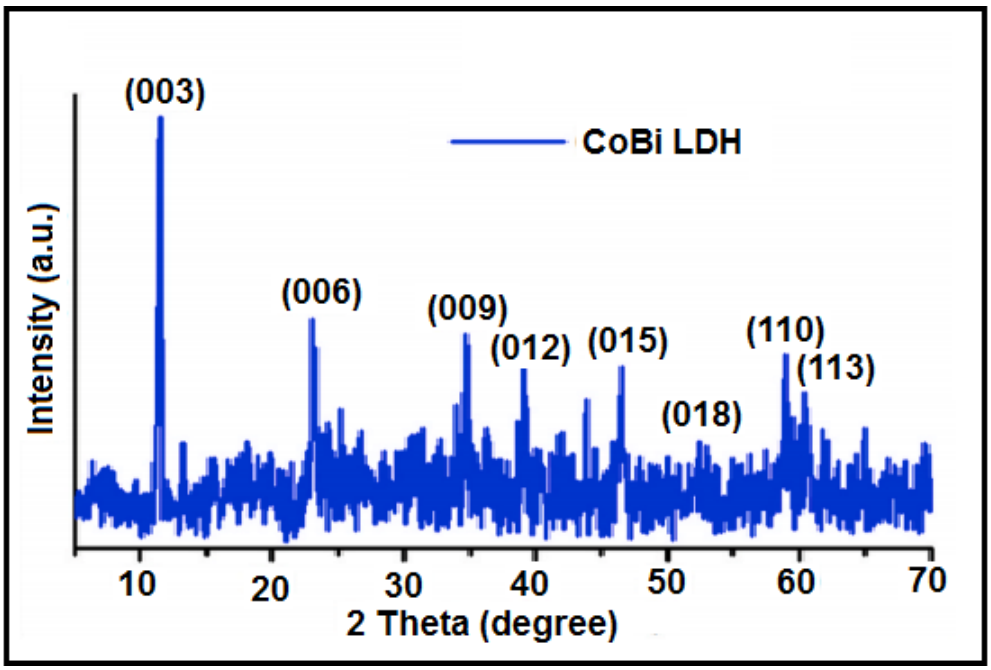

Figure 3. A typical XRD pattern of an LDH-structure; CoBi LDH [1]. Copyright 2021, reproduced with permission from Elsevier.

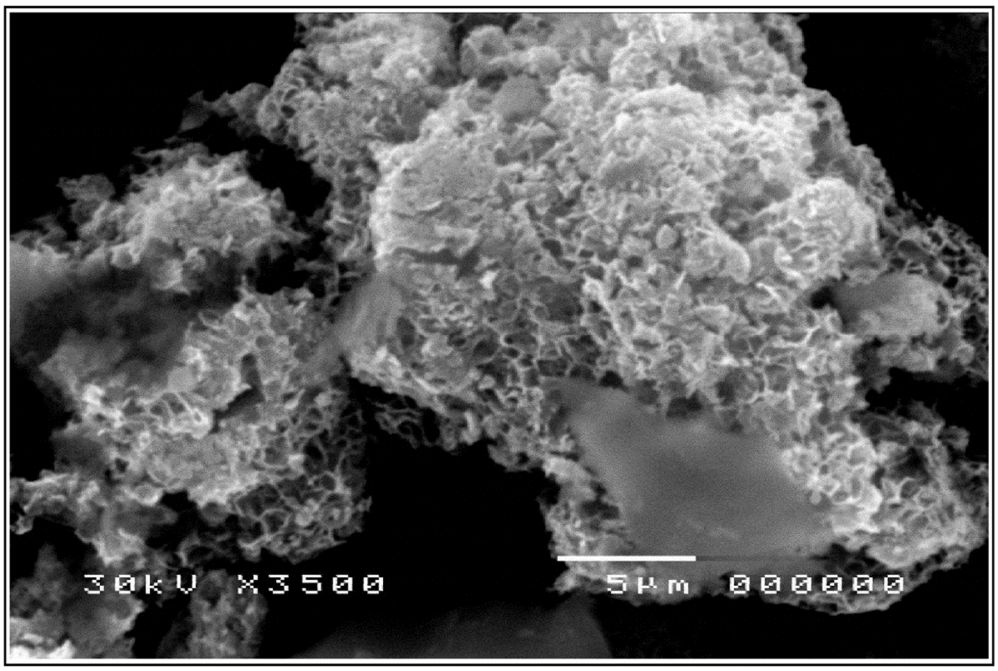

Figure 4. SEM images of lab-prepared CoMgAl LDHs [6]. Copyright 2018, reproduced with permission from the American Chemical Society.

Surface area is a common analysis of LDHs, especially in the applications of adsorption, where it plays a predominant role in the sorption of different ions. Table 1 shows the surface areas of various LDHs; it is very variable and dramatically alters with the used preparation method of the LDH, the M^{II}/M^{III} ratio, and the metal type.

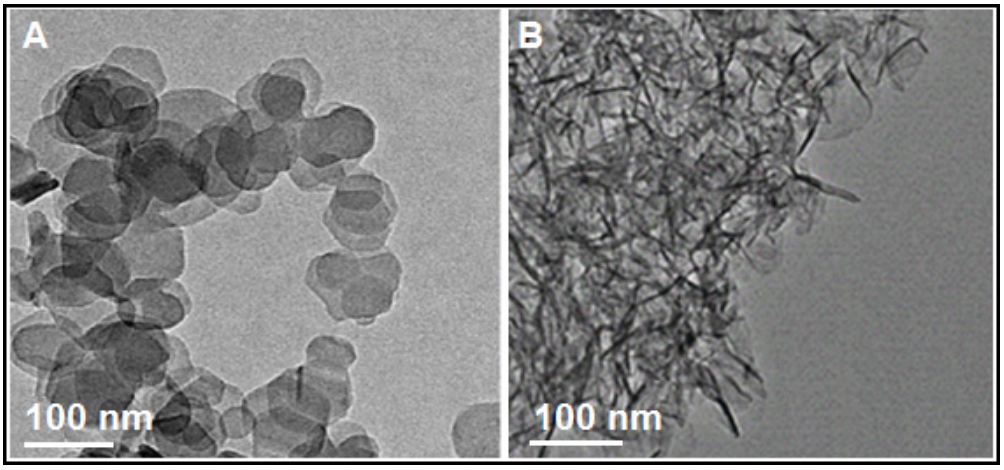

Figure 5. HRTEM images of (**A**) MgAl LDH and (**B**) $NiCo^{+3}$ Fe-LDH [63]. Copyright 2020, reproduced with permission from Elsevier.

6. Applications of LDHs in the Petroleum Industry

6.1. LDHs/LDH-Based Materials as Hydrotreating Catalysts

An Ni-enriched mixed oxide (Ni-MMO) derived from NiAl-LDH was prepared and applied as an upgrading catalyst of heavy oil at 425 °C, at a pressure of 20 bar and a catalyst/oil ratio of 0.02. Compared to the conventional NiAl-catalyst, the prepared Ni-MMO enhanced the hydrogenation reaction and yielded lighter fractions of lowered viscosities and reduced sulfur contents [65]. The results were attributed to the high surface area of the prepared NiAl-LDH, which facilitated the good distribution of the Ni-active site.

According to Wang et al. [89], novel hydrotreating catalysts of NiS_x/NiO_x and MoS_x/MoO_x were prepared by low-temperature calcination of thiomolybdate-intercalated NiAl LDH at 300 °C and applied for dibenzothiophene (DBT)-hydrodesulphurization. Compared to the conventional NiAlMo-catalyst, the prepared phases showed duplicated HDS activities, which are related to a higher Ni-promotion activity by the formation of more coordinative unsaturated sites by the mild calcination of the LDH at 300 °C. As mentioned in Section 5.2., the calcination of LDHs usually yields oxides of high surface areas, porosities, and acid/base properties.

Linares et al. [90] and his coworkers could prepare highly effective hydrotreating (HT) and hydrodesulphurization (HDS) catalysts by the facile impregnation of Co and Mo on a calcined CoNiZnAl LDH precursor. The study discussed the effect of M^{2+} to M^{3+} ratios in the CoNiZnAl LDH on the HT and HDS reactions, where the catalyst of M^{3+}/M^{3+} M^{2+} = 0.25 was more effective for the HDS of thiofene, while the catalyst of M^{3+}/M^{3+} M^{2+} = 0.33 exhibited better performance in the HT-reactions of cyclohexane.

The effect of two preparation methods on the HDS and HT activities of tungstate-intercalated NiAlZr derived catalysts was studied [91]. According to the author, the introducion of Zr by the ion-exchange method enhanced the dispersion of $NiWO_4$ and, in-turn, the reducibility and sulfidation affinities. As a result, the HDS and HT of DBT were enhanced by increasing the Zr/Al ratio to 0.3/0.7 (higher HDS activity by 55.7% compared to Zr-free catalysts).

Different catalysts of NiWAl, NiMoAl, and NiWMoAl compositions were prepared by the ion exchanging of intercalated terephthalate with heptamolybdate (Mo_7O_{246}-) and/or metatungstate ($H_2W_{12}O_{406}$-) and then calcination and sulfidation at 250 at 340 °C, respectively. Compared to conventional catalysts of the same composition, these LDH-derived catalysts showed much higher HT and HDS activities of tetrahydronaphthalene and DBT, respectively, due to the enhanced sulfidation of Ni, W, and Mo by the LDH structure [92]. The LDH structure facilitated the sulfidation of Ni, Mo, and W species by their distribution on the LDH-surfaces.

Noble metal-free catalysts based on NiLaMgAl-LDHs were fabricated by Q. Liu et al. [93] and his research group for effective hydrogenation of heavy petroleum resin (PR) to hydro-treated PR as a valuable product. The introduction of La into the synthesized LDHs enhanced both Ni reducibility and dispersion (reduced particle size), in addition to increasing the bulk-basicity for better long-chain bond cleavage. The prepared Ni/La-containing catalysts showed a hydrogenation efficiency of about 96%, with stable structural and catalytic activity over 100 h.

6.2. LDHs/LDH-Based Materials as Oxidative Desulfurization Catalysts

A recent work by Song et al. [94] discussed the aerobic oxidative desulfurization of model organosulfur compounds (BT, DBT, DMDBT) by (CoFeMo)-oxide catalysts derived from the calcination of Mo-intercalated CoFe-LDHs at 500 °C. The calcination of Mo/CoFe LDH yielded different phases, comprising Co_3O_4, Fe_3O_4, $CoFe_2O_4$, $FeMoO_4$, $CoMoO_4$, β $FeMoO_4$, and β $CoMoO_4$ of various Co, Fe, and Mo oxidation states and catalytic activities. Full aerobic oxidation of DBT was possible at 120 °C after about 20 min, while the full oxidation of the model organosulfur compounds by the Mo-containing catalysts was in the following order: 4,6 dimethydibentothiofene (DMDBT) > DBT > BT at T = 100 °C. Gao et al. [95] could prepare a new LaZnAlMo-LDH photocatalyst with La/Zn/Al ratios = 1/7/2 by the urea hydrolysis method for the UV-desulphurization of BT in diesel oil. According to this work, Mo was introduced to the LDH by the ion exchanging of CO_3^{2-}-intercalated LaZnAl LDH with Cl^- and then replacing the Cl^- ions with Mo by the immersion of Cl^-LaZnAl LDH in Na_2MoO_4 for 30 min at 80 °C. Practically, the prepared photocatalyst achieved BT-photodegradation of 87% after 2 h of irradiation. The introduction of MoO^{2-} lowered the bandgap energy from 5.12 (of CO_3^{2-} intercalated LDH) to 3.85 and 1.27 eV of La intercalated LDHs. The ZnAl-LDH nanostructure of variable surface/interlayer defects enhanced the photocatalytic activity of the guest species by the quenching of excited charges as well as the high distribution of the photocatalyst particles in the photodegradation process.

Visible light photocatalytic oxidative desulfurization of DBT in gasoline model fuel was performed by NiFe, NiCo, and CoFe intercalated with CO_3^{2-} as a guest anion. According to the study [96], a maximum DBT-removal of 76% was achieved by the prepared NiCo LDH/Fe_3O_4 photocatalyst after 222 min. The oxidation mechanism is shown in Figure 6. Efficient desulphurization and denitrogenation of model oil of S-content = 1000 ppm and N_2-content of 100 ppm were achieved by novel polyoxymetalate (POMs) that were intercalated. Experimentally, the catalyst of the Tris-LDH-LaW10 structure could reduce the S-content to 10 ppm and the N_2-content to 1 ppm through ultra-deep desulfurization and denitrogenation at 65 °C [97]. The mesoporous structure of the prepared LDHs was attributed to fast e-/h transfer and photocatalytic enhancement. The advanced synergy between MOF-76 on CaMgAl LDH was constructed by Siqi Liu [98] and his co-workers for the deep desulfurization of BT, DBT, and 4,6 DMDBT at low temperatures (60 °C). Experimentally, complete removal of the S-compounds was achieved after 25, 40, and 55 min, respectively, and the catalyst of 49% MOF-67/LDH exhibited much higher desulfurization activity (100%) than pure MOF-67, LDH, or (MOF-67 + LDH)-mix.

6.3. LDHs/LDH-Based Materials as Adsorbents for Petroleum Hazards

Due to the intrinsic properties of LDHs, such as high surface areas, porosities, and interlayer vacancies, they are widely applied as active adsorbents for petroleum and organic pollutants. According to S. Lee et al. [99], CoFe-LDH with Co/Fe = 3:1 was prepared by the co-precipitation method and used as an H_2S-adsorbent under high humid conditions. At a humid atmosphere = 90%, the prepared LDH-adsorbent achieved a high adsorption capacity of 0.209 g H_2S/g by surface intermediate HS produced from the dissociation of H_2S or by the reaction of it with the interlayered carbonate species. The LDH-adsorbent exhibited a stable adsorptive affinity, even at a high S-concentration (3333 ppm), with the formation of CO_2-gas and solid CoFeS/$CoFeSO_4$ products.

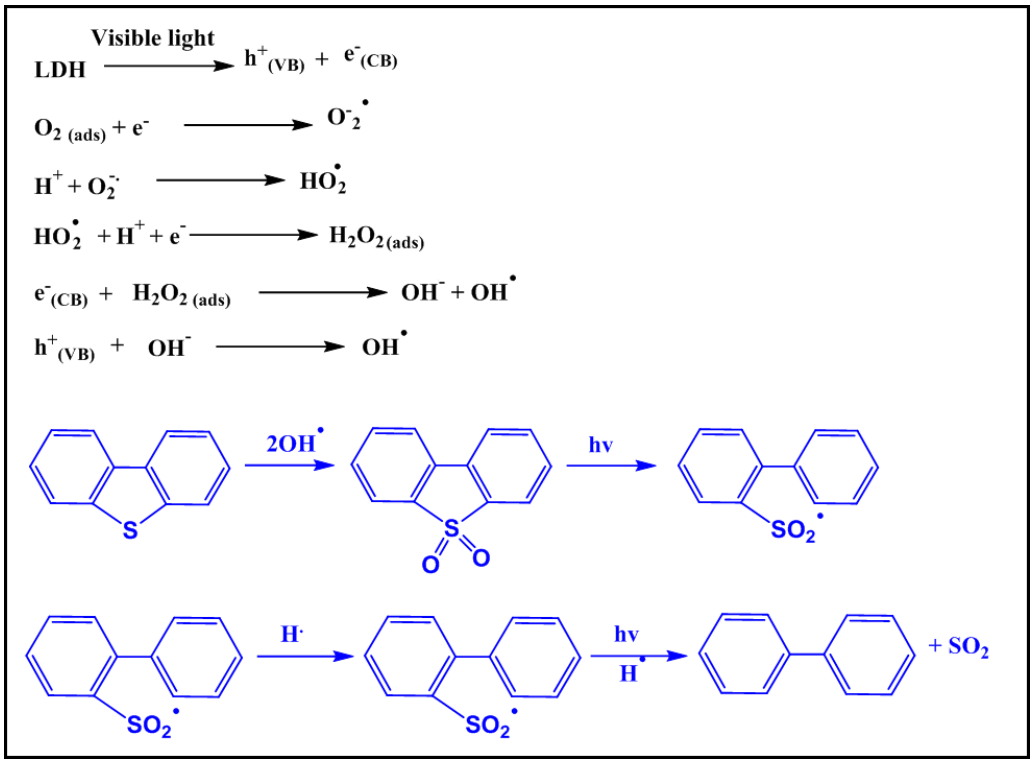

Figure 6. The photo-desulfurization mechanism over the ($NiCo_2$-LDH/Fe_3O_4)-composite. (Adopted from Masoumi and Hosseini [96], with permission from Elsevier).

A research work by R. Menzel et al. [100] discussed the preparation and impregnation of mixed metal oxides (MMO) of MgAl, CuAl, and CoAl LDHs on graphene oxide (GO) for the adsorption removal of DBT from the liquid phase at 50 °C. It was found that MgAl-MMO/GO showed the higher adsorption capacity of 1.45 mg S/g adsorbent, where GO acted as a dispersant (spacer) for the adsorbed species to the LDH.

Carbonate-intercalated MgAl LDHs with Mg/Al = 2:1 and 4:1 were prepared and applied for the SO_2 sorption at 140, 170, and 200 °C. In the gas phase, adsorption of SO_2 and the removal of SO_2 decreased by increasing the Mg ratio from 2 to 4. Conventional $Ca(OH)_2$ exhibited higher SO_2-removal, while the adsorption was found to proceed through the interaction of SO_2 and the interlayered carbonate in the LDH adsorbents [101]. This reflects the effective role of the interlayer anions of LDHs in the adsorptive and catalytic processes by the possible interaction with targeted pollutants.

6.4. LDHs/LDH-Based Materials as Petroleum Additives

LDHs possess multi-layered structures of hybrid organic and inorganic groups; the layers allow great mobilities of the LDH-structure, while the organic groups can effectively interact with the covalent bonds of organic compounds. This feature encourages the applications of LDHs for improvement of the rheological and anti-friction properties of heavy petroleum cuts.

The rheological properties and aging resistance of bitumen were improved by the incorporation of surface organic modified LDH material. According to C. Zhang et al. [102], the effect of both MgAl(CO_3^{2-})-LDH and surface-modified MgAl(CO_3^{2-})-LDH with propyltrimethoxysilane (KH560) was applied to molten bitumen at 170 °C and subjected to UV-irradiation. The experiments showed that KH560-LDH could enhance the physical properties of bitumen. involving the rheological and aging resistance. higher than KH560-modified bitumen or LDH-modified bitumen.

Sodium dodecyl sulfate (SDS) intercalated La/MgAl LDH was synthesized and applied as an antifriction agent of lube oil. According to the published study [103], the

SDS-intercalated LDH of La/Al molar ratio = 0.1 showed the highest tribological property compared to the pure La/MgAl-LDH. The results were attributed to the good dispersion of the nanoparticles in the lube media and the increase in the layers of lamellar spaces by the SDS-organic layers.

According to a European patent [104], a monolayer of LDH could be prepared by the inverse emulsion method and applied for enhanced oil recovery, where the prepared LDH-monolayer showed elevated emulsifying properties.

Great enhancement in the tribological properties of grease-based lube oil was reached by 1 wt.% LDH-additive of composition of Co/Mg/Zn/Ni LDH. According to H. Wang et al. [105], the LDH sample of a great surface area (139 m^2g^{-1}) could lower the wear to only 0.2% due to the reaction between LDH-additives and the lube oil-sliding solid surface.

6.5. LDHs for Sensing and Photodegradation of Organic Compounds

Different NiCo LDH nanocomposites of 3D flower-like morphologies were prepared and applied for the detection of toxic NO_2 gas at room temperature. According to L. He et al. [106], the composite of Co:Ni of a molar ratio = 1:1 exhibited the highest response (31.22) at 100 ppm, with a fast response and recovery time of 1.6 s and 11.6 s, respectively. The sensing activity of the prepared LDH was related to the high surface area and the synergy between $Co(OH)_2$ and $Ni(OH)_2$.

Zhang et al. [107] studied the synergy between Mn-substitution and oxygen-vacancies in the photodegradation of toluene as a model of volatile organic compounds (VOC) under visible light irradiation. ZnAl LDH was firstly prepared and then subjected to substitution with Mn to prepare MnxZnAl composites, where x = 0, 0.25, 0.5, 0.75, and 1. The photocatalyst of $Mn_{0.5}$ZnAl LDH showed the highest photodegradation activity of 97% after 180 min, where the Mn concentration could lower the conduction band edge by sufficient oxygen vacancies.

The photodegradation of many volatile organic compounds, such as benzene, ortho, meta, and Para xylenes, occurred over ZnCr-LDH and Au/ZnCr-LDH at different performance conditions. Including relative humidity, catalyst mass, initial concentration, and irradiation intensity. Experimentally, Au-containing ZnCr-LDH showed enhanced photodegradation towards the mentioned organic compounds (~84% removal for ortho-xylene at 35 °C and 50% humidity) due to the enhanced charge transfer between the Au-nanoparticles and the LDH-layers, in addition to the LDH-hydroxide groups [108].

6.6. LDHs/LDH-Based Materials for Removal of Oil Wastewater

Due to the long-dependence on crude oil as a major source of energy in the last decades, a huge amount of oil-wastewater was produced from the various oil-processing steps and especially those related to oil drilling systems. The estimated oil-wastewater counts are about 250 million barrels per day, containing different organic hazards, such as sulfonated lignite of abundant functional groups, such as sulfonic acid, phenolic, hydroxyl, carboxyl, and ketone groups [109]. Sulfonated lignite is classified as a very hazardous material to humans and the environment, since it is a catching agent of heavy metals and pesticides/herbicides, and it can increase their concentration in water. Sulfonated lignite is widely used in the oilfield as a viscosity/fluid loss reducer for freshwater drilling fluids, because of its good dispersibility and low viscosity. Accordingly, the problem of sulfonated lignite must not be left without proper handling.

LDHs have a high content of (OH)-groups along their layered structures of high surface areas and, in turn, high affinities towards the water molecules in petroleum or as free water.

A rare work describing the role of hierarchical MgAl-LDH in the adsorptive removal of sulfonated lignite was recently published by Zhou et al. [109]. The material was hydrothermally synthesized in the presence of CTAB/salicylic acid as directing agents to produce flower/worm-like morphologies of a high surface area and mesoporous structure. Accordingly, the prepared hierarchical MgAl-LDH achieved an elevated adsorption

capacity of 1014.20 mg/g at 25 °C and an initial pH of 7, which was much higher than the conventional MgAl-LDH (86 mg/g), following a pseudo second-order kinetics model and Freundlich isotherm.

Zeolite A (ZA), MgAl LDH, and ZA/MgAl LDH were prepared and applied for the removal of both cationic (Al, Cd, Cu, Mn, Ni, Pb, and Zn) and anionic (Cl, Br, NO_3, CN, SO_4, and PO_3) contaminants from oil-wastewater [110]. The prepared materials achieved an adsorption removal that varied from 80 to 100% of cations and from 60 to 100% for the different anions.

7. LDHs/LDH-Based Materials for Water Treatment

7.1. Adsorption of Heavy Metals

The effective adsorptive removal of Pb (II) from an aqueous solution was performed by Mg_2AL-LDH, Mg_3Al-LDH, and glutamate-intercalated MgAl-LDH. It was found that the glutamate-intercalated Mg_2Al-LDH reached a maximum Pb adsorption capacity of 68.5 mg/g following a Pseudo-second-order kinetic model through the Langmuir monolayer adsorption mechanism [111]. A published work by R. Soltani et al. [112] discussed the removal of Hg and Ni heavy metals by NiCo LDH, functionalized COOH/triamino-NiCo LDH, UiO-66-(Zr)-$(COOH)_2$, and the nanocomposite mixture of them. The LDH/MOF nanocomposite achieved an adsorption removal of 509.8 mg g^{-1} for Hg (II) and 441.0 mg·g^{-1} for Ni (II).

Different LDH-based adsorbents comprising MgAl, MgFe, $[SnS_4]^{4-}$/MgFe, and $[SnS_4]^{4-}$/MgAl LDHs were synthesized and applied for the adsorptive removal of Hg(II) and As(III) at different experimental conditions [113]. Among the prepared materials, the $[SnS_4]^{4-}$/MgFe LDH-adsorbent showed the highest adsorption removal of 99% towards both Hg(II) and As(III). The adsorption and photodegradation of Cr (VI) were performed by Bi-intercalated ZnAl-LDH [91]. The adsorption removal of Cr(VI) reached 84% by Bi_5O_7I/ZnAlBi-CLDH for 60 min, while the same LDH could reach 98% removal of Cr by the photodegradation under visible light irradiation.

The adsorption of Cr (VI) in the form of potassium dichromate from an aqueous solution was performed by two LDH-adsorbents: NiFe-LDH and glycerol (GL)-NiFe LDH [114]. The introduction of glycerol was found to increase the adsorption capacity to 136 mg/g compared to 50.43 mg/g of the pure NiFe-LDH, due to a preferred interaction between the dichromate ions with GL urea and LDH. A Zn_2Cr-LDH adsorbent was synthesized by the co-precipitation method and applied for the removal and recovery of pyrophosphate (PP) from electroplating wastewater [115]. At 1 g/L adsorbent, initial PP concentration = 50 mg/L, pH = 6, and adsorption time course of 6 h, the removal efficiency of PP by Zn_2Cr-LDH reached 86%. The LDH-adsorbent also showed good reusability and recovery of the adsorbed PP when treated with NaOH.

The removal of soil heavy metals, such as Cu, Pb, Zn, and Ni, was performed by 3D- Vermiculite-supported Mg-Al (LDH@VMT) [116]. It was found that the adsorption of Cu and Pb was through precipitation by the LDH-hydroxide groups, where the removal of Zn and Ni was conducted by amorphous replacement. A concurrent adsorption of methylene blue (MB) and Pb (II) and Hg (II) was investigated by M. Chen et al. [117] using sodium polyacrylate-MgAl LDH adsorbents (PAAS-LDH). At a neutral pH, initial ion concentration of 50 mg/L, adsorbent load = 0.1 g/L, and T = 40 °C, the prepared PAAS-LDH adsorbent could reach adsorption capacities of 211 mg/g for MB, 345.4 mg/g for Pb (II), and 142.7 mg/g for Hg (II) Hg through possible complex-formation between the adsorbed metals and the LDH-carboxylate groups.

7.2. Removal of Industrial Dyes

According to recent reports, the dye-market involves 1×10^4 different types, the worldwide dye-production is huge (7×10^5 tons/year), and 15% of the produced dyes directly contaminate the drinking water [118]. Due to their specific organic structure, the industrial dyes are classified as very toxic compounds to humans, plants, the eco-system,

animals, and marine life. Accordingly, many separations and treatment techniques are applied to handle the problem of dye-release to the ecosystem, such as micro-filtration, ultra-filtration, nano-filtration, reverse osmosis, photodegradation, oxidation, and adsorption. The adsorption of dyes finds wide applications due to its feasibility compared to other routes, while LDHs appear as highly active materials in this sector; the following section cites some of the applied LDH-adsorbents in dye-removal.

The effect of temperature, adsorption time, pH, and concentration on the adsorption of (Acid Yellow 42)-dye by fresh/calcined MgAl(CO_3^{2-})-LDH was studied by R.M.M. Santos et al. [119]. The authors showed that the calcined MgAl LDH could enhance the adsorption removal of the (Acid Yellow 42)-dye by four times: 1266 $mg \cdot g^{-1}$ at room temperature and pH = 7 compared to 330 $mg \cdot g^{-1}$ by the fresh MgAl LDH at the same conditions. The authors attributed the results to the memory effect phenomena of the calcined MgAl LDH. Different NiFeTi LDH-adsorbents of different Ti-ratios were prepared and applied for very fast adsorption of MO, MB, Congo red (CR), and Orange G (OG) dyes from contaminated wastewater [120]. The prepared materials could achieve very fast removal of the different dyes (90% within 2 min) due to the high surface areas and the available -OH/CO_3^{2-} groups in the prepared LDHs.

The parallel adsorption of cationic/anionic dyes and heavy metals by a carbon-LDH composite (C/Ca_xAlMg LDH) was investigated by Sukanya Kundu and Milan Kanti Naskar [121]. According to the authors, the prepared materials possessed high surface areas (477–758 m^2g) to achieve maximum adsorption capacities of 122.1 and 328.95 mg/g for MB and MO, respectively. The removal of organic MB and MO dyes by zeolite imidazolate frameworks/CoAl LDH composite was investigated by M.A. Nazir, et al. [122]. Experimentally, the ZIF-67@CoAl-LDH adsorbent showed an elevated adsorption capacity towards MB (57.24 mg/g) compared to pure CoAl-LDH (15 mg/g) or pure ZIF-67 (57.14 $mg \cdot g^{-1}$). In the adsorption removal of MO, the composite also achieved a much higher adsorption capacity (180.5 mg/g) than bare adsorbents.

Optically-responsive CoNiTi-LDH synthesized by a hydrothermal route was applied for the photodegradation of cationic/anionic dyes from an aqueous solution [123]. Experimentally, the prepared photocatalyst showed much better removal towards both Rhodamine B (∼99.8%) and Acid Red G (∼99.6%) compared to commercial catalysts, such as CoO, NiO, or TiO_2, due to the sufficient radical generation, excellent charge-separation, high surface areas, and the low bandgap energy (2.6 eV) of the LDH-photocatalyst. Diatoms (DE)-modified MgAl-LDHs (DE-LDHs) were prepared and applied for the removal of Congo Red (CR). The incorporation of the LDH into the diatoms sharply increased their surface area from 28 to 51 m^2/g and increased the maximum (CR)-removal efficiency from ~15% of DE-adsorbent to ~98% by the DE-LDH adsorbents [124].

A promising (Zn/Al LDH/biochar)-composite was synthesized by liquid deposition treatment for the adsorptive removal of MB in an aqueous solution under different conditions, such as initial concentration, adsorption time, pH medium, and temperature. The (Zn/Al-LDH/biochar)-composite showed higher surface area properties (58.461 m^2/g) than ZnAl-LDH (9.621 m^2/g) or biochar (50.936 m^2/g) to achieve the maximum (MB)-removal of 59% at pH = 5 and 60 °C [125]. Environmental remediation by upgrading petroleum was investigated early through the effective adsorptive removal of organo-sulfur compounds from petroleum wax [6,121] as a common heavy byproduct. A highly surface-active CoMo LDH was synthesized and applied as a novel adsorbent for sulfur from wax-distillate. According to the study, a refined micro crystalline wax for medical and other purposes was obtained by a cost-effective technique via using CoMo LDH-adsorbent [126], where the high surface area of the prepared LDH-adsorbent of the highly charged surface and porosity played the essential role in adsorption of the organic contaminants as sulfur from wax.

8. The Recent Breakthrough in Synthesis and Applications of 1D LDHs

The fast progress and development of the world civilization in the last decades led to severe climate changes and threatened millions of people. The elevating earth temperature and ocean acidity dramatically threaten the coastal cities through abnormal floods and extreme rains. These climate changes can also result in world food shortage and uncontrolled starvations. The year 2021 recorded the highest greenhouse gas rates, with abnormal floods, extreme rainfalls, and dangerous wildfires in many parts of Europe, Asia, and north America [127]. By the end of October 2021, the world meteorological organization (WMO, Geneva) reported that the available solutions to protect our humanity against these climate changes should be through world cooperation to encourage the global production and dependence on hydrogen instead of fossil fuels [1,6]. Hydrogen is a perfect energy carrier; it can be generated and used in green routes, has a high caloric value, and can be produced from renewable sources [1,6,128]. However, the production of hydrogen globally is still facing implemental crises due to the wide bandgap energies of the current semiconductors and their main operation in the UV-region of only 5% of the solar light.

In 2014, Li and his coworkers [1,6] led a motivating attempt to overcome the restricted working of semiconductors in the UV-region by assuming the boron nitride photocatalyst as infrared (IR)-responsive. The IR-radiation accounts for about 54% of sunlight and is available in the day, night, and cloudy conditions. Although, the proposed IR-responsive achieved low hydrogen evolution rates (HERs). Following the leading Li's negotiation, we could discover 1D LDHs in 2020 as highly active and potentially IR-responsive for enhanced photocatalytic water-splitting reactions [70]. Firstly, we could prepare 1D CoTi LDH for enhanced IR-induced water oxidation by a one-pot urea hydrolysis route depending on chloride-based precursors. The chloride-based synthesis led to 1D-propagation (Figure 7) through the formation of a $[TiO_6]^{2-}$ intermediate. The prepared 1D CoTi LDH showed a typical IR-bandgap of 1.4 eV (Figure 8), with bandgap positions suitable for water oxidation to O_2, which is the challenging half-reaction in the process. In the water-splitting process, 1D CoTi LDH could achieve an HER of 5300 $\mu molg^{-1} \cdot h^{-1}$ under 200-watt irradiation at 50 °C without any promoters or scavengers (Figure 9). The 1D-assembly increased the (CoTi LDH)-distribution in water, IR-absorbance and transferring, and the short pathway for the electrons/holes pairs. Due to the containing surface and interlayer water, carbonate, and cyanate groups, 1D CoTi LDH could dramatically quench the photoexcited species and prevent their fast recombination instead of using organic or inorganic scavengers.

For the first time, cyanate intercalated CoBi LDH could be prepared in a 1D-assembly as highly active IR-responsive in a potential trial to prepare one that is feasibly IR-responsive with high photocatalytic water-splitting activities. The prepared photocatalyst showed the highest oxidation states of Bi and Ti (according to the XPS measurements), as well as the lowest bandgap value of the CoBi-structure (1.32 eV). Accordingly, 1D CoBi LDH achieved the highest OER of 5300 $\mu molg^{-1}h^{-1}$, where the predominant cyanate groups effectively captured the photoexcited species and offered a shorter pathway for their migration into the photocatalyst surface [1].

Since hydrogen production by photocatalytic water splitting is an urgent and great world goal, we fabricated the first IR-structure for this purpose in 2022 by constructing a novel 3D CoBiTi LDH/CoBiTi LDO heterojunction (Figure 10) for the first time [127]. The CoBiTi LDH (CBT-LDH) was firstly prepared in 1D-morphology with excellent visible light responsivity (bandgap = 2.3 eV) to achieve an HER of ~273 $\mu molg/g/h$ as the highest HER under IR-irradiation. The assembly of highly active Co, Bi, and Ti elements in nanorod (1D)-morphology greatly enhanced the chemical/photochemical properties of the CBT-LDH semiconductor by the presence of most of the atoms on the surface. This indeed increases the photocatalyst distribution and the IR-light absorbance and transferring for enhanced HER without external promoters. The 1D CBT-LDH semiconductor was easily oxidized to the corresponding 2D-CoBiTi layered double oxide (CBT-LDO) by mild drying at 150 °C. The fast oxidation at lower temperatures is attributed to the presence of most of the atoms on the outer surface of the material [77], due to the ultrathin sheets of CBT-LDH in this

case. The CBT-LDO involved highly photoactive phases of the Co_3O_5-spinel, $Bi_{12}TiO_{20}$, and $Bi_4Ti_3O_4$ [5] and could reach an HER of 113 µmol/g/h by the lowest bandgap energy value of a CoBiTi-structure: 1.27 eV.

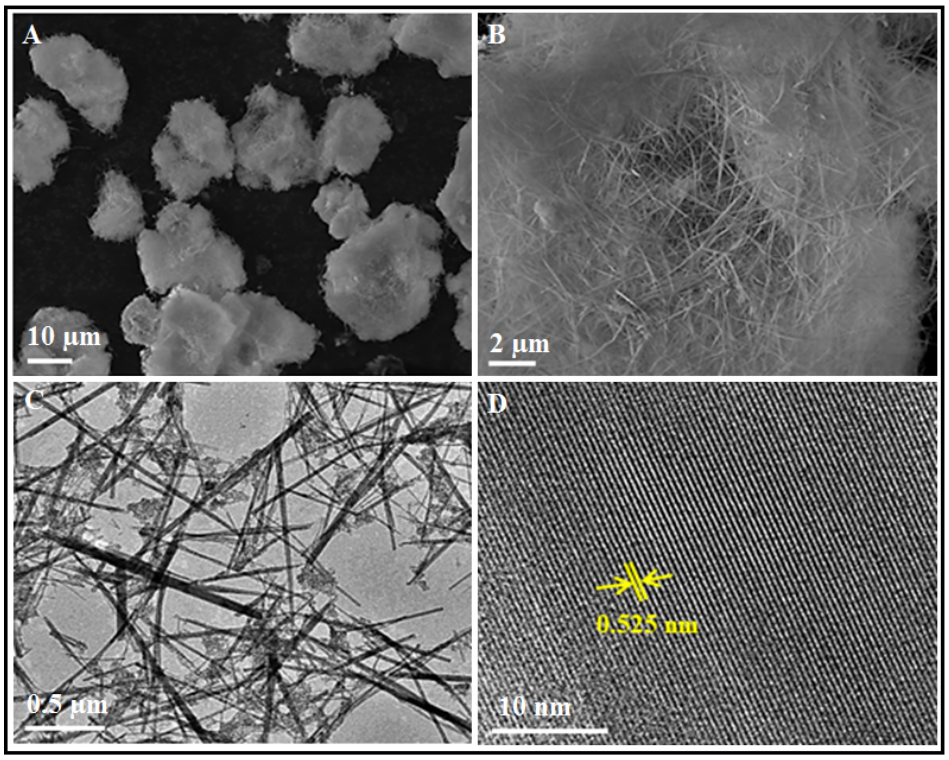

Figure 7. (**A**,**B**) SEM images and (**C**,**D**) TEM and crystal lattice of the 1D-assembly of CoTi-LDH IR-responsive for OER.

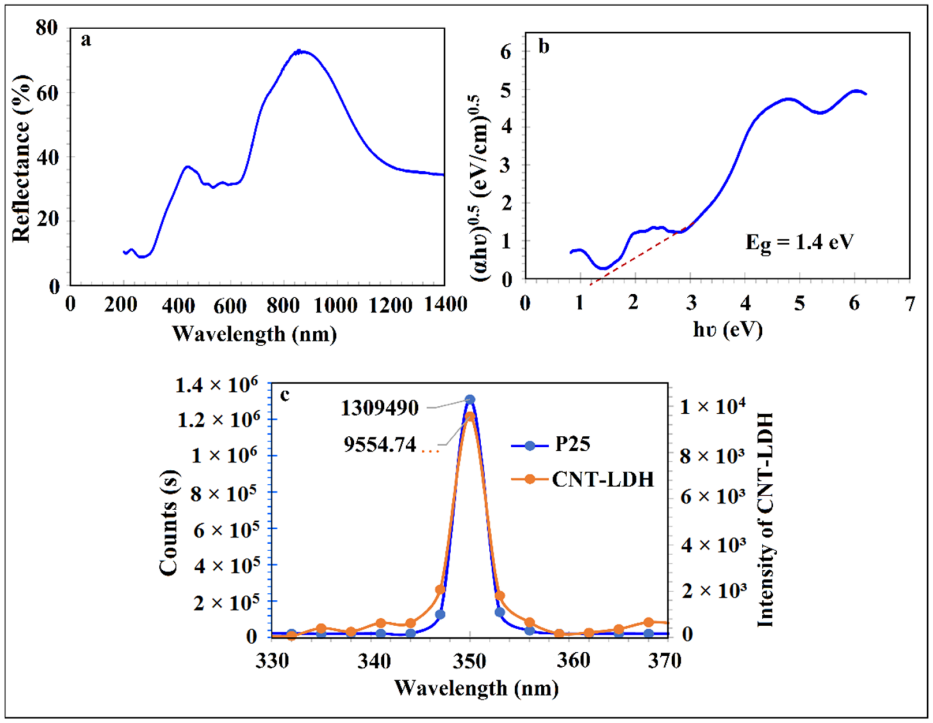

Figure 8. (**a**,**b**) The typical IR-responsivity of CoTi-LDH and (**c**) the corresponding PL compared to conventional P25.

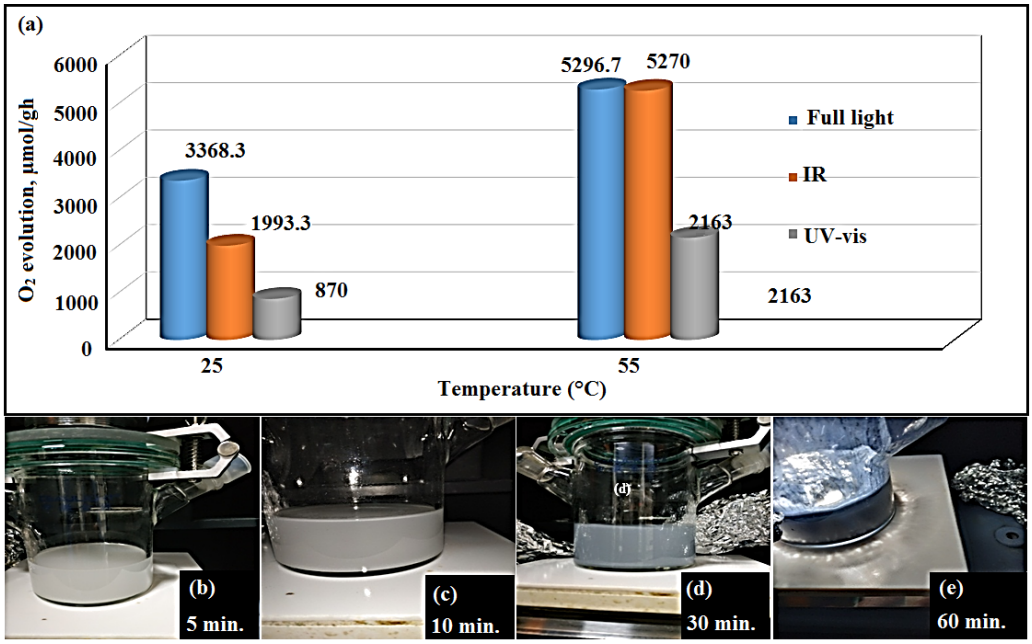

Figure 9. The photocatalytic activity of (**a**) CoTi-LDH in water splitting and (**b**–**e**) the reduction of Ag-ions by the photocatalyst at 10–60 min under IR-irradiation.

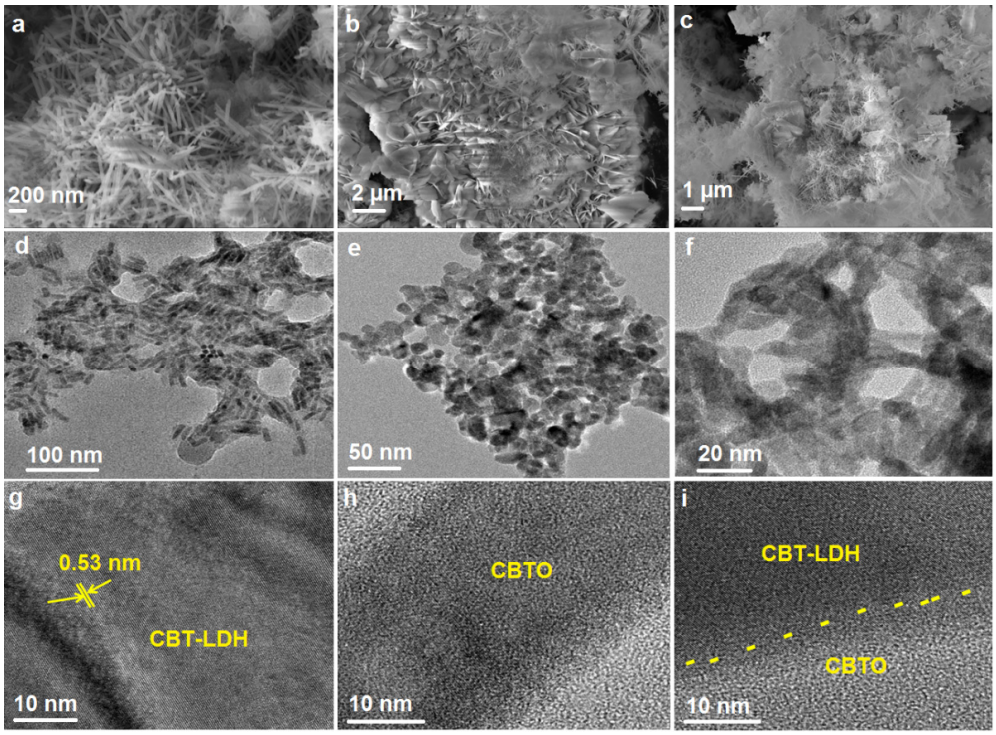

Figure 10. The surface structure/heterojunction of the prepared CBT/CBTO semiconductors [108]. The images express (**a**–**c**) SEM, and (**d**–**f**) HRTEM captures of CBT-LDH, CBTO, and the CBT-LDH/CBTO photocatalysts. The images (**g**–**i**) the crystal lattice fringes of the synthesized photocatalysts. Copyright 2022, reproduced with permission from Elsevier.

The highest HER by the abundant IR-energy, which is available all of the day and in the cloudy conditions, was possible by our previous work when we fabricated the novel 3D LDH/LDO heterojunction. It is a practical and potential pathway to increase the HER by IR energy through the mixing of CBT-LDH and CBT-LDO powders instead of going so far and preparing complex IR-structures. The novel 3D LDH/LDO led to the formation of

a type I heterojunction by two different visible lights (CBT-LDH), and it was IR-responsive and could increase the HER by five-fold (1255 µmol/g/h) (Figure 11).

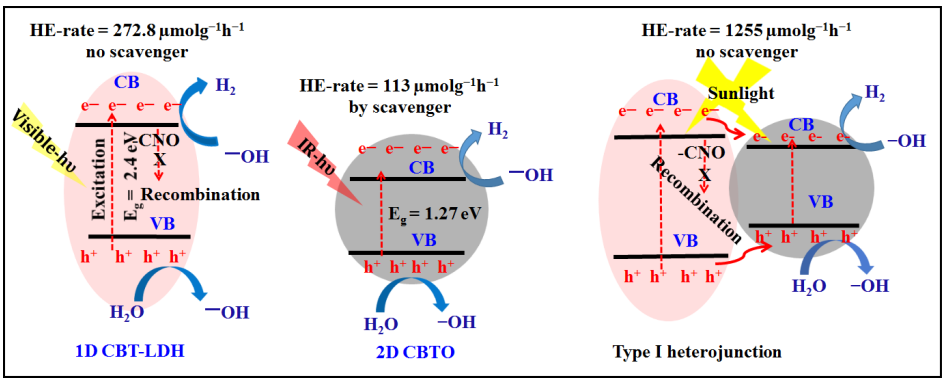

Figure 11. The role of 1D CBTO LDH in enhancing the HER of CBT-LDH by five-fold under IR-irradiation [127]. Copyright 2022, reproduced with permission from Elsevier.

In this heterojunction, the cyanate groups of CBT-LDH completely quenched the photoexcited species and allowed their migration to the surface of CBT-LDO for the reduction of H^+ to H_2 [6]. The great world goal is to get a green and renewable energy source, such as hydrogen, and introducing the IR-region in this direction is very essential to reach this goal; it is the predominant energy in the globe (sunlight). Accordingly, the 1D LDHs are the promising semiconductors to achieve the world goal of their own unique characteristics, such as high IR-responsivities, feasible preparation procedures, and availabilities of their precursors and the variable bandgap energy values from the visible to IR regions. We would like to encourage and direct the researchers in the world towards the synthesis and applications of 1D LDHs for better clean energy production and environmental remediation. Table 2 shows the quantum yield efficiency (QYE) and the effectiveness of CBT and CBTO IR-responsiveness [129–137] in the solar-to-hydrogen process compared to conventional photocatalysts. Figure 12 exhibits the CB/VB potentials of common LDHs compared to ordinary oxide photocatalysts. We cannot forget or overcome the tangential role of LDHs in other fields of energy production as the important photoelectrochemical process [138–142], although we dream, as the entire world, to get clean and renewable sources of energy without external driving forces, except the sun.

Table 2. Quantum yield efficiencies (QYE) of common photocatalysts and the effectiveness of IR-responsiveness in the solar-to-hydrogen process [127–137].

LDH-Photocatalyst	Conditions	HER ($\mu molg^{-1}h^{-1}$)	QYE	Ref.
CBT-LDH	Xe-200 W, <800 nm	272.8	-	[127]
CBT-LDH/CBTO	Xe-200 W, <800 nm	1255	-	[127]
CdS/ZnCr-LDH	Xe-340 W, <420 nm	374	42.6 (420 nm)	[129]
NiO/$NaTaO_3$:La	Hg-400 W, full light	19,800	56 (420 nm)	[130]
Pt-$Cd_{0.5}Zn_{0.5}S$:Bi	Hg-400 W, >420 nm	55.9	9.7 (420 nm)	[131]
Ni-CdS	Xe-300 W, >420 nm	25.8	26.8 (420 nm)	[132]
Pt-$La_5Ti_2AgS_5O_7$	Xe-300 W, >420 nm	225	1.2 (420 nm)	[133]
Pt-$LaInS_2O$	Xe-300 W, >420 nm	9	0.2 (420 nm)	[134]
P_3HT/g-C_3N_4	Xe-300 W, >420 nm	3045	77.4 (420 nm)	[135]
g-C_3N_4/N-rich-CNF	Xe-300 W, >420 nm	169	14.3 (420 nm)	[136]
CdS-Au-HCNS Pt	Xe-300 W, >455 nm	277	8.7 (420 nm)	[137]

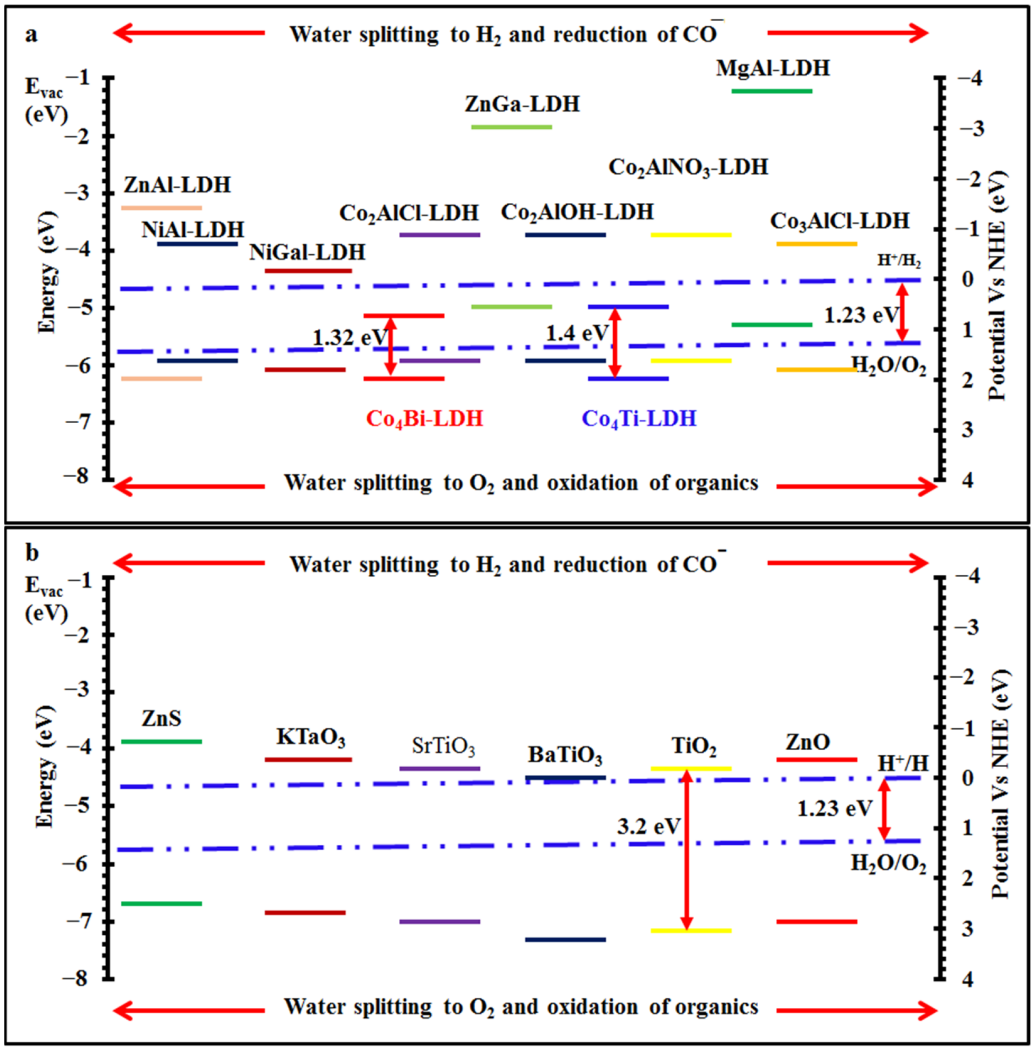

Figure 12. The CB/VB potentials of common LDHs (**a**) compared to those of conventional metal oxide photocatalysts (**b**); it is obvious how the LDH-structure can greatly improve the photocatalytic properties and lower the bandgap energies.

9. Durability of LDHs as Potential Photocatalytic Materials

According to our investigations [1,6,73,126,127], all the synthesized and applied LDH-photocatalysts exhibited stable structures in the photocatalytic water splitting under different light irradiation energies. Generally, LDHs are highly stable materials, due to the perfect asymmetry and strong bonding of the interlayer anion (CO_3^{2-}, -CN, . . .) inside the layers; this makes it so difficult to substitute the interlayer anion except by applying special treatment. To perform anion exchange to the interlayer anion, it requires immersing the LDH in a solution with a high concentration of an interfering anion at a high temperature and stirring for a long time to achieve anion exchange. For example, the recently discovered CoTi, CoBi, and CoBiTi LDH photocatalysts showed great structural stabilities with respect to the primary hydrotalcite structure (XRD) as well as the existence of the interlayer CO_{23}- and CN anions (by FTIR) after many cycles of photocatalytic water splitting [1,73,127]. LDHs usually comprise heavy metals in their structures, and the recovery of LDHs needs no complex separation methods, just settling, filtration, and drying at room temperature overnight or at 120 °C for 2–6 h. Thus, LDHs usually possess their unique crystallinities and main properties even after long use in aqueous solutions.

10. Summary and Future Prospective

Layered double hydroxides (LDHs) are well-known as hydrotalcites or anionic clay minerals with 2D multilayered structures and can intercalate different anions in contrast to the conventional cationic clay minerals, such as zeolites. LDHs possess specific excellent properties, such as the memory effect, acid–base nature, high surface area, and layer-by-layer (LBL)-assembly. Accordingly, LDHs find wide applications in the research and industrial fields, such as catalysts, photocatalysts, catalyst-supports, adsorbents, drug delivery systems, polymer nanocomposites, and additives. There have been numerous published works (research articles or reviews) discussing the applications of LDHs in the energy and environmental fields, as in the case of water splitting, green energy production, adsorption, and photodegradation of environmental pollutants. However, no relevant work has stated the application of LDHs in the petroleum field, according to our best knowledge. This review discussed the recent advancement and applications of LDHs in petroleum with respect to using LDHs as hydrotreating catalysts, catalysts for the oxidative desulfurization process, adsorbents for petroleum hazards, petroleum additives (especially for lube oil as a vital petroleum fraction), and as sensors and photocatalysts for organic compounds released from the petroleum combustion. Additionally, the introduced review stated the recent LDH-modification and applications in water treatment in respect to the removal of heavy metals from drinking water and the adsorption/photodegradation of industrial dyes of a huge world production, and very dangerous toxicities in petroleum (oil)-wastewater.

Due to the outstanding properties of LDHs, more research work is needed to widen their applications in the petroleum and petrochemical industries and to teach the synthesis methods for recently qualified things that can work in diverse fields of research and industry. It is recommended to advance LDH nanosheets, nanoclusters, and bandgap-engineered LDHs and scale-up their usage in petroleum, oil-wastewater, and other environmental fields. Additionally, the exfoliation of LDHs structure into a few layers and single sheets can expose more surface sites because of the large interlayer spacing between individual layers in the LDH structure. However, the synthesis of exfoliated NiFe-LDHs nanosheets requires complex multistep process, such as hydrothermal process, anion exchange, and exfoliation, which take several days to get the final product. Developing an effective strategy to exfoliate bulk NiFe-LDHs into stable single-layer NiFe-LDHs nanosheets with more exposed active sites remains challenging.

Funding: This work was funded by the National Key R&D program of China (No. 2021YFA1202804).

Data Availability Statement: Data can be available upon request from the authors.

Acknowledgments: This work was supported by the National Center for Nanoscience and Technology (NCNST), 11 Zhongguancun Beiyitiao, Haidian District, Beijing, 100190, China; Egyptian Petroleum Research Institute, Nasr City, Cairo 11727, Egypt, and Guangdong University of Technology, Guangzhou 510006, China.

Conflicts of Interest: The authors declare no conflict of interest.

Abbreviations

LDH: Layered Double Hydroxide; eV: Electrovolt; UV: Ultraviolet; IR: Infrared; 1D: One dimensional; D2: Two dimensional; D3: Three dimensional; SOx: Sulfur Oxides; NOx: Nitrogen Oxides; ppm: Part per million; WMO: World Metrological Organization; COP26: Conference of the Parties no 26; CNT: Carbon; nanotubes; CB: Conduction band; VB: Valence band; IUPAC: International Union of Pure and Applied Chemistry; LbL: Layer-by-layer; XRD: X-ray diffraction; JCPDS: Joint Committee on Powder Diffraction Standards; SEM: Scanning electron microscopy; HRTEM: High resolution transmission electron microscope; MOF: Metal organic framework; CBT-LDH: CoBiTi LDH: CBTO: CoBiTi Oxide.

References

1. Mostafa, M.S.; Chen, L.; Selim, M.S.; Betiha, M.A.; Zhang, R.; Gao, Y.; Zhang, S.; Ge, G. Novel cyanate intercalated CoBi layered double hydroxide for ultimate charge separation and superior water splitting. *J. Clean. Prod.* **2021**, *313*, 127868. [CrossRef]
2. Chen, G.; Lin, J.; Hu, W.; Cheng, C.; Gu, X.; Du, W.; Zhang, J.; Qu, C. Characteristics of a crude oil composition and it's in situ waxing inhibition behavior. *Fuel* **2018**, *218*, 213–217. [CrossRef]
3. Coutinho, D.M.; França, D.; Vanini, G.; Gomes, A.O.; Azevedo, D.A. Understanding the molecular composition of petroleum and its distillation cuts. *Fuel* **2022**, *311*, 122594. [CrossRef]
4. Mostafa, M.M.; El Saied, M.; Morshedy, A.S. Novel Calcium Carbonate-titania nanocomposites for enhanced sun light photo catalytic desulfurization process. *J. Environ. Manag.* **2019**, *250*, 109462. [CrossRef]
5. Li, Y.; Dang, L.; Han, L.; Li, P.; Wang, J.; Li, Z. Iodine-sensitized Bi_4Ti3O_{12}/TiO_2 photocatalyst with enhanced photocatalytic activity on degradation of phenol. *J. Mol. Catal. A Chem.* **2013**, *379*, 146–151. [CrossRef]
6. Mostafa, M.S.; Betiha, M.A.; Rabie, A.M.; Hassan, H.M.; Morshedy, A.A. New conduct in the adsorptive removal of sulfur compounds by new nickel-molybdenum adsorbent. *Ind. Eng. Chem. Res.* **2018**, *57*, 425–433. [CrossRef]
7. Luca, C.G.; Aguire, M.H.; Selli, E. Hydrogen production by photocatalytic steam reforming of methanol on noble metal-modified TiO_2. *J. Catal.* **2010**, *273*, 182–190.
8. Istiroyah; Engge, Y.; Maulana, F.; Nurhuda, M. Literature review of the development of ZnO and TiO_2 as photocatalytic material in water splitting processes. In Proceedings of the 11th International Conference on Global Resource Conservation, East Java, Indonesia, 28–29 July 2020.
9. Li, Y.; Wang, G.; Zhang, H.; Qian, W.; Li, D.; Guo, Z.; Zhou, R.; Xu, J. Hierarchical flower-like 0D/3D g-C_3N_4/TiO_2 S-scheme heterojunction with enhanced photocatalytic activity. *Coll. Surf. A Physicochem. Eng. Asp.* **2022**, *646*, 128942. [CrossRef]
10. Ayyub, M.M.; Chhetri, M.; Gupta, U.; Roy, A.; Rao, C.N.R. Photochemical and Photoelectrochemical Hydrogen Generation by Splitting Seawater. *Chem. Eur. J.* **2018**, *24*, 18455–18462. [CrossRef] [PubMed]
11. Song, C.; Yin, C.; Qu, H. Electronic microstructure and thermal conductivity modeling of semiconductor nanomaterials. *Microelectr. J.* **2021**, *108*, 104988. [CrossRef]
12. Nur, A.S.M.; Sultana, M.; Mondal, A.; Islam, S.; Robel, F.N.; Islam, A.; Sumi, M.S.A. A review on the development of elemental and codoped TiO_2 photocatalysts for enhanced dye degradation under UV-vis irradiation. *J. Water Process Eng.* **2022**, *47*, 102728. [CrossRef]
13. Esrafili, A.; Salimi, M.; Jafari, A.; Sobhi, H.R.; Gholami, M.; Kalantary, R.R. Pt-based TiO_2 photocatalytic systems: A systematic review. *J. Mol. Liq.* **2022**, *352*, 118685. [CrossRef]
14. Feng, L.; Li, B.; Xiao, Y.; Li, L.; Zhang, Y.; Zhao, Q.; Zuo, G.; Meng, X.; Roy, V.A.L. Au modified Bi_2O_3-TiO_2 hybrid for photocatalytic synthesis of hydrogen peroxide. *Catal. Commun.* **2021**, *155*, 106315. [CrossRef]
15. Cruz, D.; Ortiz-Oliveros, H.B.; Flores-Espinosa, R.M.; Pérez, P.Á.; Ruiz-López, I.I.; Quiroz-Estrada, K.F. Synthesis of Ag/TiO_2 composites by combustion modified and subsequent use in the photocatalytic degradation of dyes. *J. King Saud Univ. Sci.* **2022**, *34*, 101966. [CrossRef]
16. Ti, J.; Zhu, J.; He, B.; Zong, Z.; Yao, X.; Tui, R.; Huang, H.; Chen, C.; Chen, H.; Duan, Y.; et al. A "double-sided tape" modifier bridging the TiO2/perovskite buried interface for efficient and stable all-inorganic perovskite solar cells. *J. Mater. Chem. A* **2022**, *10*, 6649–6661. [CrossRef]
17. Zhao, H.; Yu, X.; Li, C.-F.; Yu, W.; Wang, A.; Hu, Z.-Y.; Larter, S.; Li, Y.; Kibria, M.G.; Hu, J. Carbon quantum dots modified TiO_2 composites for hydrogen production and selective glucose photoreforming. *J. Energy Chem.* **2022**, *64*, 201–208. [CrossRef]
18. Suligoj, A.; Arcon, I.; Mazaj, M.; Drazic, G.; Arcon, D.; Cool, P.; Stangar, U.L.; Tusar, N.N. Surface modified titanium dioxide using transition metals: Nickel as a winning transition metal for solar light photocatalysis. *J. Mater. Chem. A* **2018**, *6*, 9882–9892. [CrossRef]
19. Xie, Z.; Liu, X.; Zhan, P.; Wang, W.; Zhang, Z. Tuning the optical bandgap of TiO_2 -TiN composite films as photocatalyst in the visible light. *AIP Adv.* **2013**, *3*, 062129. [CrossRef]
20. Guidetti, G.; Pogna, E.A.A.; Lombardi, L.; Tomarchio, F.; Polishchuk, I.; Joosten, R.R.M.; Ianiro, A.; Soavi, G.; Sommerdijk, N.A.J.M.; Friedrich, H.; et al. Photocatalytic activity of exfoliated graphite -TiO_2 nanoparticle composites. *Nanoscale* **2019**, *11*, 19301–19314. [CrossRef]
21. Yao, J.; Zhang, Y.; Wang, Y.; Chen, M.; Huang, Y.; Cao, J.; Ho, W.; Lee, S.C. Enhanced photocatalytic removal of NO over titania/hydroxyapatite (TiO_2/HAp) composites with improved adsorption and charge mobility ability. *RSC Adv.* **2017**, *7*, 24683. [CrossRef]
22. Urkasame, K.; Yoshida, S.; Takanohashi, T.; Iwamura, S.; Ogino, I.; Mukai, S.R. Development of TiO_2- SiO_2 photocatalysts having a microhoneycomb structure by the ice templating method. *ACS Omega* **2018**, *3*, 14274–14279. [CrossRef] [PubMed]
23. Widiyandari, H.; Umiati, N.A.K.; Herdianti, R.D. Synthesis and photocatalytic property of Zinc Oxide ZnO fine particle using flame spray pyrolysis method. *IOP Conf. Ser. J. Phys. Conf. Ser.* **2018**, *1025*, 012004. [CrossRef]
24. Chen, L.; Xiang, Q.; Liao, Y.; Zhang, H. CdS-Based photocatalysts. *Energy Environ. Sci.* **2018**, *11*, 1362–1391. [CrossRef]
25. Adhikari, S.; Sarkar, D.; Madras, G. Hierarchical design of CuS architectures for visible light photocatalysis of 4-Chlorophenol. *ACS Omega* **2017**, *2*, 4009–4021. [CrossRef] [PubMed]
26. Warsi, M.F.; Bilal, M.; Zulfiqar, S.; Khalid, M.U.; Agboola, P.O.; Shakir, I. Enhanced visible light driven photocatalytic activity of MnO_2 nanomaterials and their hybrid structure with carbon nanotubes. *Mater. Res. Express* **2020**, *7*, 105015. [CrossRef]

27. Wei, J.; Qu, R.; Xu, S.; Chen, J.; Al-Basher, G.; Li, C.; Shada, A.; Dar, A.A.; Wang, Z. Alumina-mediated photocatalytic degradation of hexachlorobenzene in aqueous system: Kinetics and mechanism. *Chemosphere* **2020**, *257*, 127256.
28. Kamil, N.; El Amrani, M.K.; Benjelloun, N.; Naturforsch, Z. New silica supported titanium dioxide catalysts: Characteristics and photocatalytic efficiency in waste water depollution. *Z. Naturforschung* **2006**, *61*, 1311–1318. [CrossRef]
29. Li, C.; Zhu, N.; Yang, S.; He, X.; Zheng, S.; Sun, Z.; Dionysiou, D.D. A review of clay based photocatalysts: Role of phyllosilicate mineral in interfacial assembly, microstructure control and performance regulation. *Chemosphere* **2021**, *273*, 129723. [CrossRef]
30. Dubey, N.; Rayalu, S.S.; Labhsetwar, N.K.; Devotta, S. Visible light active zeolite-based photocatalysts for hydrogen evolution from water. *Int. J. Hydrogen Energy* **2008**, *33*, 5958–5966. [CrossRef]
31. Sajid, M.M. Nanomaterials: Types, proper ties, recent advances, and toxicity concerns. *Environ. Sci. Health* **2022**, *25*, 100319.
32. Lang, J.; Takahashi, K.; Kubo, M.; Shimada, M. Preparation of TiO_2-CNT-Ag ternary composite film with enhanced photocatalytic activity via plasma-enhanced chemical vapor deposition. *Catalysts* **2022**, *12*, 508. [CrossRef]
33. Amin, M.A.; Mersal, G.A.M.; Shaltout, A.A.; Badawi, A.; El-Sheshtawy, H.S.; Das, M.R.; Boman, J.; Ibrahim, M.M. Non-covalent functionalization of graphene oxide-supported 2-Picolyamine-based zinc (II) complexes as novel electrocatalysts for hydrogen production. *Catalysts* **2022**, *12*, 389. [CrossRef]
34. Li, Y.; Xu, H.; Ouyang, S.; Ye, J. Metal—Organic frameworks for photocatalysis. *Phys. Chem. Chem. Phys.* **2016**, *18*, 7563–7572. [CrossRef] [PubMed]
35. Alduhaish, O.M.; Shaik, M.R.; Adil, S.F. Photo-Induced preparation of Ag@MOF-801 composite based heterogeneous nanocatalyst for the production of biodiesel. *Catalysts* **2022**, *12*, 533. [CrossRef]
36. Errahmani, K.B.; Benhabiles, O.; Bellebia, S.; Bengharez, Z.; Goosen, M.; Mahmoudi, H. Photocatalytic nanocomposite polymer-TiO_2 membranes for pollutant removal from wastewater. *Catalysts* **2021**, *11*, 402. [CrossRef]
37. Omr, H.A.E.; Horn, M.W.; Lee, H. Low-dimensional nanostructured photocatalysts for efficient CO_2 conversion into solar fuels. *Catalysts* **2021**, *11*, 418. [CrossRef]
38. Qin, Q.; Wang, J.; Xia, Y.; Yang, D.; Zhou, Q.; Zhu, X.; Feng, W. Synthesis and characterization of Sn/Ni single doped and co-doped anatase/rutile mixed-Crystal nanomaterials and their photocatalytic performance under UV-Visible Light. *Catalysts* **2021**, *11*, 1341. [CrossRef]
39. El Hakim, S.; Chave, T.; Nikitenko, S.I. Photocatalytic and Sonocatalytic Degradation of EDTA and Rhodamine B over Ti0 and Ti@TiO Nanoparticles. *Catalysts* **2021**, *11*, 928. [CrossRef]
40. Prasad, C.; Tang, H.; Liu, Q.Q.; Zulfiqar, S.; Shah, S.; Bahadur, I. An overview of semiconductors/layered double hydroxides composites: Properties, synthesis, photocatalytic and photoelectrochemical applications. *J. Mol. Liq.* **2019**, *289*, 111114. [CrossRef]
41. Zhao, Y.; Zhang, S.; Shi, R.; Waterhouse, G.I.N.; Tang, J.; Zhang, T. Two-dimensional photocatalyst design: A critical review of recent experimental and computational advances. *Mater. Today* **2020**, *34*, 78–91. [CrossRef]
42. Zhao, Y.; Waterhouse, G.I.N.; Chen, G.; Xiong, X.; Wu, L.-Z.; Tung, C.-H.; Zhang, T. Two-dimensional-related catalytic materials for solar-driven conversion of COx into valuable chemical feedstocks. *Chem. Soc. Rev.* **2019**, *48*, 1972–2010. [CrossRef]
43. Sun, X.; Huang, H.; Zhao, Q.; Ma, T.; Wang, L. Thin-Layered Photocatalysts. *Adv. Funct. Mater.* **2020**, *30*, 1910005. [CrossRef]
44. Sun, X.; Shi, L.; Huang, H.; Song, X.; Ma, T. Surface engineered 2D materials for photocatalysis. *Chem. Commun.* **2020**, *56*, 11000–11013. [CrossRef] [PubMed]
45. Williams, G.R.; O'Hare, D. Towards understanding, control and application of layered double hydroxide chemistry. *J. Mater. Chem.* **2006**, *16*, 3065–3074. [CrossRef]
46. Mohapatra, L.; Parida, K. A review on the recent progress, challenges and perspective of layered double hydroxides as promising photocatalysts. *J. Mater. Chem. A* **2016**, *4*, 10744–10766. [CrossRef]
47. Yan, K.; Wu, G.; Jin, W. Recent advances in the synthesis and applications of layered double hydroxide-based materials and their applications in hydrogen and oxygen evolution. *Energy Technol.* **2016**, *4*, 354–368. [CrossRef]
48. Zhao, Y.; Jia, X.; Waterhouse, G.I.N.; Wu, L.-Z.; Tung, C.-H.; O'Hare, D.; Zhang, T. Layered double hydroxide nanostructured photocatalysts for renewable energy production. *Adv. Energy Mater.* **2016**, *6*, 1501974. [CrossRef]
49. Nishimura, S.; Takagaki, A.; Ebitani, K. Characterization, synthesis and catalysis of hydrotalcite-related materials for highly efficient materials transformations. *Green Chem.* **2013**, *15*, 2026–2042. [CrossRef]
50. Xu, M.; Wei, M. Layered double hydroxide-based catalysts: Recent advances in preparation, structure and applications. *Adv. Funct. Mater.* **2018**, *28*, 802943. [CrossRef]
51. Lu, X.; Xue, H.; Gong, H.; Bai, M.; Tang, D.; Ma, R.; Sasaki, T. 2D Layered double hydroxide nanosheets and their derivatives toward efficient oxygen evolution reaction. *Nano-Micro Lett.* **2020**, *12*, 86. [CrossRef] [PubMed]
52. Fan, G.; Li, F.; Evans, D.G.; Duan, X. Catalytic applications of layered double hydroxides: Recent advances and perspectives. *Chem. Soc. Rev.* **2014**, *43*, 7040–7066. [CrossRef] [PubMed]
53. Yang, Z.; Wang, F.; Zhang, C.; Zeng, G.; Tan, X.; Yu, Z.; Zhong, Y.; Wang, H.; Cui, F. Utilization of LDH-based materials as potential adsorbents and photocatalysts for the decontamination of dyes wastewater: A review. *RSC Adv.* **2016**, *6*, 79415–79436. [CrossRef]
54. Wu, M.J.; Wu, J.Z.; Zhang, J.; Chen, H.; Zhou, J.Z.; Qian, G.R.; Xu, Z.P.; Du, Z.; Rao, Q.L. A review on fabricating heterostructures from layered double hydroxides for enhanced photocatalytic activities. *Catal. Sci. Technol.* **2018**, *8*, 1207–1228. [CrossRef]
55. Yang, Z.Z.; Zhang, C.; Zeng, G.-M.; Tan, X.-F.; Wang, H.; Huang, D.-L.; Yang, K.-H.; Wei, J.-J.; Ma, C.; Nie, K. Design and engineering of layered double hydroxide based catalysts for water depollution by advanced oxidation processes: A review. *J. Mater. Chem. A* **2020**, *8*, 4141–4173. [CrossRef]

56. Razzaq, A.; Ali, S.; Asif, M.; In, S.-I. Layered double hydroxide (LDH) based photocatalysts: An outstanding strategy for efficient photocatalytic CO_2 conversion. *Catalysts* **2020**, *10*, 1185. [CrossRef]
57. Ng, S.F.; Lau, M.Y.L.; Ong, W.J. Engineering layered double hydroxide—Based photocatalysts toward artificial photosynthesis: State-of-the-art progress and prospects. *Sol. RRL* **2021**, *5*, 2000535. [CrossRef]
58. Wang, Y.; Yan, D.; El Hankari, S.; Zou, Y.; Wang, S. Recent progress on layered double hydroxides and their derivatives for electrocatalytic water splitting. *Adv. Sci.* **2018**, *5*, 1800064. [CrossRef] [PubMed]
59. Cavani, F.; Trifiro, F.; Vaccari, A. Hydrotalcite-type anionic clays: Preparation, properties and applications. *Catal. Today* **1991**, *11*, 173–302. [CrossRef]
60. Mochane, M.J.; Magagula, S.I.; Sefadi, J.S.; Sadiku, E.R.; Mokhena, T.C. Morphology, thermal stability, and flammability properties of polymer-layered double hydroxide (LDH) nanocomposites: A review. *Crystals* **2020**, *10*, 612. [CrossRef]
61. Wijitwongwan, R.; Intasa-ard, S.; Ogawa, M. Preparation of Layered Double Hydroxides toward Precisely Designed Hierarchical Organization. *ChemEngineering* **2019**, *3*, 68. [CrossRef]
62. Tian, R.; Liang, R.; Wei, M.; Evans, D.J.; Duan, X. Applications of layered double hydroxide materials: Recent advances and perspective. *Struct. Bond.* **2015**, *430*, 205.
63. Chen, J.; Wang, C.; Zhang, Y.; Guo, Z.; Luo, Y.; Mao, C.J. Engineering ultrafine NiS cocatalysts as active sites to boost photocatalytic hydrogen production of MgAl layered double hydroxide. *Appl. Surf. Sci.* **2020**, *506*, 144999. [CrossRef]
64. Gonçalves, J.M.; Martins, P.R.; Angnes, L.; Araki, K. Recent advances in ternary layered double hydroxide electrocatalysts for the oxygen evolution reaction. *New J. Chem.* **2020**, *44*, 9981–9997. [CrossRef]
65. Johnston, A.M.; Lester, E.; Williams, O.; Gomes, R.L. Understanding layered double hydroxide properties as sorbent materials for removing organic pollutants from environmental waters. *J. Environ. Chem. Eng.* **2021**, *9*, 105197. [CrossRef]
66. Wu, L.; Pan, F.; Liu, Y.; Zhang, G.; Tang, A.; Atrens, A. Influence of pH on the growth behaviour of Mg-Al LDH films. *Surf. Eng.* **2018**, *34*, 674–681. [CrossRef]
67. Zhao, Y.; Xiao, F.; Jiao, Q. Hydrothermal synthesis of Ni/Al layered double hydroxide nanorods. *J. Nanotechnol.* **2011**, *11*, 646409. [CrossRef]
68. Iqbal, M.A. Effect of synthesis conditions on the controlled growth of MgAl–LDH corrosion resistance film: Structure and corrosion resistance properties. *Michele Fedel Coat* **2019**, *9*, 30. [CrossRef]
69. Li, G.; Zhang, J.; Li, L.; Yuan, C.; Weng, T.C. Boosting the electrocatalytic activity of nickel-iron layered double hydroxide for the oxygen evolution reaction by terephthalic acid. *Catalysts* **2022**, *12*, 258. [CrossRef]
70. Nayak, S.; Parida, K. MgCr-LDH nanoplatelets as effective oxidation catalysts for visible light-triggered Rhodamine B degradation. *Catalysts* **2021**, *11*, 1072. [CrossRef]
71. Agostino, L.C.D.; Gonçalves, R.G.L.; Santilli, C.V.; Pulcinelli, S.H. Effect of solvent in the sol-gel synthesis of layered double hydroxides as catalysts for the ethanol steam reforming reaction. In Proceedings of the 18. Brazil MRS Meeting, Balneario Camboriu, Brazil, 22–26 September 2019.
72. Zhao, Y.; He, S.; Wei, M.; Evans, D.G.; Duan, X. Hierarchical films of layered double hydroxides by using a sol-gel process and their high adaptability in water treatment. *Chem. Commun.* **2010**, *46*, 3031–3033. [CrossRef]
73. Mostafa, M.S.; Lan, C.; Betiha, M.A.; Zhang, R.; Gaoa, Y.; Ge, G. Enhanced infrared-induced water oxidation by one-pot synthesized CoTi-Nanorods as highly infrared responsive photocatalyst. *J. Power Source* **2020**, *464*, 228176. [CrossRef]
74. Chowdhury, P.R.; Bhattacharyya, K.G. Synthesis and characterization of Co/Ti layered double hydroxide and its application as a photocatalyst for degradation of aqueous Congo Red. *RSC Adv.* **2015**, *5*, 92189–92206. [CrossRef] [PubMed]
75. Chowdhury, P.R.; Bhattacharyya, K.G. Ni/Ti layered double hydroxide: Synthesis, characterization and application as a photocatalyst for visible light degradation of aqueous methylene blue. *Dalton Trans.* **2015**, *44*, 6809–6824. [CrossRef]
76. Chen, G.; Qian, S.; Tu, X.; Wei, X.; Zou, J.; Leng, L.; Luo, S. Enhancement photocatalytic degradation of rhodamine B on nano Pt intercalated Zn–Ti layered double hydroxides. *Appl. Surf. Sci.* **2014**, *293*, 345–351. [CrossRef]
77. Xia, J.Y.; Tang, M.T.; Chen, C.; Jin, S.M.; Chen, Y.M. Preparation of α-Bi_2O_3 from bismuth powders through low-temperature oxidation. *Trans. Nonferrous Metals Soc. China* **2012**, *22*, 2289–2294.
78. Li, C.D.; Li, M.; van Veen, A.C. Chapter 1—Synthesis of Nano-catalysts in flow conditions using millimixers. In *Advanced Nanomaterials, Advanced Nanomaterials for Catalysis and Energy*; Sadykov, V.A., Ed.; Elsevier: Amsterdam, The Netherlands, 2019; pp. 1–28.
79. Tichit, D.; Layrac, G.; Gérardin, C. Synthesis of layered double hydroxides through continuous flow processes: A review. *Chem. Eng. J.* **2019**, *369*, 302–332. [CrossRef]
80. Chen, Y.; Jing, C.; Zhang, X.; Jiang, D.; Liu, X.; Dong, B.; Feng, L.; Li, S.; Zhang, Y. Acid- salt treated CoAl layered double hydroxide nanosheets with enhanced adsorption capacity of Methyl Orange dye. *J. Colloid Interface Sci.* **2019**, *548*, 100–109. [CrossRef]
81. El Hassani, K.; Beakou, B.H.; Kalnina, D.; Oukani, E.; Anouar, A. Effect of morphological properties of layered double hydroxides on adsorption of azo dye Methyl Orange: A comparative study. *Appl. Clay Sci.* **2017**, *140*, 124–131. [CrossRef]
82. Guan, T.; Fang, L.; Lu, Y.; Wu, F.; Ling, F.; Gao, J.; Hu, B.; Meng, F.; Jin, X. A facile approach to synthesize 3D flower-like hierarchical NiCo layered double hydroxide microspheres and their enhanced adsorption capability. *Coll. Surf. A Physicochem. Eng. Asp.* **2017**, *529*, 907–915. [CrossRef]

83. Jiang, Z.; Yan, L.; Wu, J.; Liu, X.; Zhang, J.; Zheng, Y.; Pei, Y. Low-temperature synthesis of carbonate-intercalated NixFe-layered double hydroxides for enhanced adsorption properties. *Appl. Surf. Sci.* **2020**, *531*, 147281. [CrossRef]
84. Jing, C.; Chen, Y.; Zhang, X.; Guo, X.; Liu, X.; Dong, B.; Dong, F.; Zhang, X.; Liu, Y.; Li, S.; et al. Low carbonate contaminative and ultrasmall NiAl LDH prepared by acid salt treatment with high adsorption capacity of Methyl Orange. *Ind. Eng. Chem. Res.* **2019**, *58*, 11985–11998. [CrossRef]
85. Shabbir, R.; Gu, A.; Chen, J.; Khan, M.M.; Wang, P.; Jiao, Y.; Zhang, Z.; Liu, Y.; Yang, Y. Highly efficient removal of congo red and Methyl Orange by using petal-like Fe-Mg layered double hydroxide. *Int. J. Environ. Anal. Chem.* **2022**, *102*, 1–18. [CrossRef]
86. Chao, Y.-F.; Lee, J.-J.; Wang, S.-L. Preferential adsorption of 2,4-dichlorophenoxyacetate from associated binary-solute aqueous systems by Mg/Al-NO_3 layered double hydroxides with different nitrate orientations. *J. Hazard. Mater.* **2009**, *165*, 846–852. [CrossRef] [PubMed]
87. Zheng, Y.M.; Li, N.; Zhang, W.D. Preparation of nanostructured microspheres of Zn-Mg-Al layered double hydroxides with high adsorption property. *Coll. Surf. A Physicochem. Eng. Asp.* **2012**, *415*, 195–201. [CrossRef]
88. Lu, Y.; Jiang, B.; Fang, L.; Ling, F.; Gao, J.; Wu, F.; Zhang, X. High performance NiFe layered double hydroxide for Methyl Orange dye and Cr(VI) adsorption. *Chemosphere* **2016**, *152*, 415–422. [CrossRef]
89. Wang, H.; Fan, Q.; Yang, Z.; Tang, S.; Chen, J.; Wu, Y. A novel pre-sulfided hydrotreating catalyst derived from thiomolybdate intercalated NiAl LDHs. *Mol. Catal.* **2019**, *468*, 1–8. [CrossRef]
90. Linares, C.F.; Vásquez, M.; Castillo, R.; Bretto, P.; Solano, R.; Rincón, A. Applications of CoMo/calcined quaternary hydrotalcites for hydrotreatment reactions. *Fuel Process. Technol.* **2015**, *132*, 105–110. [CrossRef]
91. Wang, H.; Yang, Z.; Meng, F.; Yin, W.; Wu, Y. Effects of preparation methods on the property and hydrodesulfurization activity of NiAlZrW catalysts derived from tungstate intercalated NiAlZr layered double hydroxides. *Fuel* **2018**, *228*, 332–341. [CrossRef]
92. Arias, S.; Lice, Y.E.; Soares, D.; Eon, J.G.; Palacio, L.A.; Faro, A.C., Jr. Mixed NiMo, NiW and NiMoW sulfides obtained from layered double hydroxides as catalysts in simultaneous HDA and HDS reactions. *Catal. Today* **2017**, *296*, 187–196. [CrossRef]
93. Li, Q.; Yang, J.; Zhang, H.; Sun, H.; Wu, S.; Ge, B.; Wang, R.; Yuan, P. Tuning the properties of Ni-based catalyst via La incorporation for efficient hydrogenation of petroleum resin. *J. Chem. Eng.* **2022**, *45*, 41–50. [CrossRef]
94. Song, Y.; Bai, J.; Jiang, S.; Yang, H.; Yang, L.; Wei, D.; Bai, L.; Wang, W.; Liang, Y.; Chen, H. Co-Fe-Mo mixed metal oxides derived from layered double hydroxides for deep aerobic oxidative desulfurization. *Fuel* **2021**, *306*, 121751. [CrossRef]
95. Gao, L.G.; Li, H.X.; Song, X.L.; Li, W.L.; Ma, X.R. Degradation of benzothiophene in diesel oil by LaZnAl layered double hydroxide: Photocatalytic performance and mechanism. *Petrol. Sci.* **2019**, *16*, 173–179. [CrossRef]
96. Masoumi, S.; Hosseini, S.A. Desulfurization of di-benzothiophene from gasoil model using Ni-Co_2, $NiFe_2$ and Co-Fe_2 nano layered-double hydroxides as photocatalysts under visible light. *Fuel* **2020**, *277*, 118137. [CrossRef]
97. Yao, Z.; Miras, H.N.; Song, Y.F. Efficient concurrent removal of sulfur and nitrogen contents from complex oil mixtures by using polyoxometalate-based composite material. *Inorg. Chem. Front.* **2016**, *3*, 1007–1013. [CrossRef]
98. Liu, S.; Li, X.; Zhang, H. Synergistic effects of MOF-76 on layered double hydroxides with superior activity for extractive catalytic oxidative desulfurization. *New J. Chem.* **2020**, *44*, 6269–6276. [CrossRef]
99. Lee, S.; Govindan, M.; Kim, D. CoFe-based layered double hydroxide for high removal capacity of hydrogen sulfide under high humid gas stream. *Chem. Eng. J.* **2021**, *416*, 127918. [CrossRef]
100. Menzel, R.; Iruretagoyena, D.; Wang, Y.; Bawaked, S.M.; Mokhtar, M.; Al-Thabaiti, S.A.; Basahel, S.N.; Shaffer, M.S.P. Graphene oxide/mixed metal oxide hybrid materials for enhanced adsorption desulfurization of liquid hydrocarbon fuels. *Fuel* **2016**, *181*, 531–536. [CrossRef]
101. Kameda, T.; Tochinai, M.; Kumagai, S.; Yoshioka, T. Mg−Al layered double hydroxide intercalated with CO_3^{2-} and its recyclability for treatment of SO_2. *Appl. Clay Sci.* **2019**, *183*, 105349. [CrossRef]
102. Zhang, C.; Yu, J.; Xu, X.; Sun, Y. Effect of surface organic modified layered double hydroxide on UV ageing resistance of bitumen. *Pet. Sci. Technol.* **2017**, *35*, 488–494. [CrossRef]
103. Li, S.; Qin, H.; Zuo, R.; Bai, Z. Friction properties of La-doped Mg/Al layered double hydroxide and intercalated product as lubricant additives. *Tribol. Int.* **2015**, *91*, 60–66. [CrossRef]
104. Parvulescu, A.N.; Kimura, R.; Zoellner, B.; Holtze, C.; Weisse, S.A.; Lorenz, S.; Ulrich, M. Monolayer from at Least One Layered Double Hydroxide (LDH). EP 3 015 429 A1, 4 May 2016.
105. Wang, H.; Wang, Y.; Liu, Y.; Zhao, J.; Li, J.; Wang, Q.; Luo, J. Tribological behavior of layered double hydroxides with various chemical compositions and morphologies as grease additives. *Friction* **2021**, *9*, 952–962. [CrossRef]
106. He, L.; Zhang, W.; Zhang, X.; Bai, X.; Chen, J.; Ikram, M.; Zhang, G.; Shi, K. 3D flower-like NiCo-LDH composites for a high-performance NO_2 gas sensor at room temperature. *Coll. Surf. A Physicochem. Eng. Asp.* **2020**, *603*, 125142. [CrossRef]
107. Zhang, J.; Shen, B.; Hu, Z.; Zhen, M.; Guo, S.Q.; Dong, F. Uncovering the synergy between Mn substitution and O vacancy in ZnAl-LDH photocatalyst for efficient toluene removal. *Appl. Catal. B Environ.* **2021**, *296*, 120376. [CrossRef]
108. Fu, S.; Zheng, Y.; Zhou, X.; Ni, Z.; Xia, S. Visible light promoted degradation of gaseous volatile organic compounds catalyzed by Au supported layered double hydroxides: Influencing factors kinetics and mechanism. *J. Hazard. Mater.* **2019**, *363*, 41–54. [CrossRef]
109. Zhou, L.; Slaný, M.; Bai, B.; Du, W.; Qu, C.; Zhang, J.; Tang, Y. Enhanced Removal of Sulfonated Lignite from Oil Wastewater with Multidimensional MgAl-LDH Nanoparticles. *Nanomaterials* **2021**, *11*, 861. [CrossRef]

110. Bezerra, P.G.B.; Bieseki, L.; da Silva, D.R.; Pergher, S.B.C. Development of a zeolite A/LDH composite for simultaneous cation and anion removal. *Materials* **2019**, *12*, 661. [CrossRef]
111. Yanming, S.; Dongbin, L.; Shifeng, L.; Lihui, F.; Shuai, C.; Haque, M.A. Removal of lead from aqueous solution on glutamate intercalated layered double hydroxide. *Arab. J. Chem.* **2017**, *10*, 2295–2301. [CrossRef]
112. Soltani, R.; Pelalak, R.; Pishnamazi, M.; Marjani, A.; Shirazian, S. A water-stable functionalized NiCo-LDH/MOF nanocomposite: Green synthesis, characterization and its environmental application for heavy metals adsorption. *Arab. J. Chem.* **2021**, *14*, 103052. [CrossRef]
113. Li, S.; Xu, H.; Wang, L.; Ji, L.; Li, X.; Qu, Z.; Yan, N. Dual-functional sites for selective adsorption of mercury and arsenic ions in $[SnS_4]^{4-}$/MgFe-LDH from wastewater. *J. Hazard. Mater.* **2021**, *403*, 123940. [CrossRef]
114. Abo el-Reesh, G.Y.; Farghali, A.A.; Taha, M.; Mahmoud, R.K. Novel synthesis of ni/fe layered double hydroxides using urea and glycerol and their enhanced adsorption behavior for Cr(VI)removal. *Sci. Rep.* **2020**, *10*, 587. [CrossRef]
115. Fu, D.; Kurniawan, T.A.; Avtar, R.; Xu, P.; Othman, M.H.D. Recovering heavy metals from electroplating wastewater and their conversion into Zn2Cr-layered double hydroxide (LDH) for pyrophosphate removal from industrial wastewater. *Chemosphere* **2021**, *271*, 129861. [CrossRef]
116. Zhao, S.; Meng, Z.; Fan, X.; Jing, R.; Yang, J.; Shao, Y.; Liu, X.; Wu, M.; Zhang, Q.; Liu, A. Removal of heavy metals from soil by vermiculite supported layered double hydroxides with three-dimensional hierarchical structure. *Chem. Eng. J.* **2020**, *390*, 124554. [CrossRef]
117. Chen, M.; Bi, R.; Zhang, R.; Yang, F.; Chen, F. Tunable surface charge and hydrophilicity of sodium polyacrylate intercalated layered double hydroxide for efficient removal of dyes and heavy metal ion. *Coll. Surf. A Physicochem. Eng. Asp.* **2021**, *617*, 126384. [CrossRef]
118. Daud, M.; Hai, A.; Banat, F.; Wazir, M.B.; Habib, M.; Bharath, G.; Al-Harthi, M.A. A review on the recent advances, challenges and future aspect of layered double hydroxides (LDH)-Containing hybrids as promising adsorbents for dyes removal. *J. Mol. Liq.* **2019**, *288*, 110989. [CrossRef]
119. dos Santos, R.M.M.; Gonçalves, R.G.L.; Constantino, V.R.L.; Santilli, C.V.; Borges, P.D.; Tronto, J.; Pinto, F.G. Adsorption of Acid Yellow 42 dye on calcined layered double hydroxide: Effect of time, concentration, pH and temperature. *Appl. Clay Sci.* **2017**, *140*, 132–139. [CrossRef]
120. Rathee, G.; Awasthi, A.; Sood, D.; Tomar, R.; Tomar, V.; Chandra, R. Layered double hydroxide adsorbent for ultrafast removal of anionic organic dyes. *Sci. Rep.* **2019**, *9*, 16225. [CrossRef]
121. Kundu, S.; Naskar, M.K. Carbon-layered double hydroxide nanocomposite for efficient removal of inorganic and organic based water contaminants—Unravelling the adsorption mechanism. *Mater. Adv.* **2021**, *2*, 3600–3612. [CrossRef]
122. Nazir, M.A.; Khan, N.A.; Cheng, C.; Shah, S.S.A.; Najam, T.; Arshad, M.; Sharif, A.; Akhtar, S.; ur Rehman, A. Surface induced growth of ZIF-67 at Co-layered double hydroxide: Removal of methylene blue and methyl orange from water. *Appl. Clay Sci.* **2020**, *190*, 105564. [CrossRef]
123. Chowdhury, P.R.; Bhattacharyya, K.J. Ni/Co/Ti layered double hydroxide for highly efficient photocatalytic degradation of Rhodamine B and Acid Red G: A comparative study. *Photochem. Photobiol. Sci.* **2017**, *16*, 835–839. [CrossRef]
124. Sriram, G.; Uthappa, U.T.; Losic, D.; Kigga, M.; Jung, H.-Y.; Kurkuri, M.D. MgAl-layered double hydroxide (LDH) modified diatoms for highly efficient removal of congo red from aqueous solution. *Appl. Sci.* **2020**, *10*, 2285. [CrossRef]
125. Lesbani, A.; Meg, P.; Bahar, S.; Siregar, N.; Palapa, N.R.; Taher, T.; Riyanti, F. Adsorptive removal methylene-blue using Zn/Al LDH modified rice husk biochar. *Pol. J. Environ. Stud.* **2021**, *30*, 3117–3124. [CrossRef]
126. Mostafa, M.S.; Mohamed, N.H. Towards novel adsorptive nanomaterials: Synthesis of $Co^{+2}Mo^{+6}$ LDH for sulfur and aromatic removal from crude petroleum. *Egypt. J. Pet.* **2016**, *25*, 221–227. [CrossRef]
127. Mostafa, M.S.; Lan, C.; Selim, M.S.; Ruiyi, Z.; Ya, G.; Shuai, Z.; Ge, G. Synthesis of novel CoBiTi LDH and fabrication of LDH-LDO 3D-Hetero -junction for enhanced infrared induced water splitting to hydrogen. *J. Clean. Prod.* **2022**, *340*, 130663. [CrossRef]
128. Awadallah, A.; Mostafa, M.S.; Aboul-Enein, A.A.; Hanafi, S.A. Hydrogen production via methane decomposition over Al_2O_3-TiO_2 binary oxides supported Ni catalysts: Effect of Ti content on the catalytic efficiency. *Fuel* **2014**, *129*, 68–77. [CrossRef]
129. Zhang, G.; Lin, B.; Yang, W.; Jiang, S.; Yao, Q.; Chen, Y.; Gao, B. Highly efficient photocatalytic hydrogen generation by incorporating CdS into ZnCr-layered double hydroxide interlayer. *RSC Adv.* **2015**, *5*, 5823–5829. [CrossRef]
130. Kato, H.; Asakura, K.; Kudo, A. Highly efficient water splitting into H_2 and O_2 over Lanthanum-doped $NaTaO_3$ photocatalysts with high crystallinity and surface nanostructure. *J. Am. Chem. Soc.* **2003**, *125*, 3082–3089. [CrossRef]
131. Peng, S.; An, R.; Li, Y.; Lu, G.; Li, S. Remarkable enhancement of photocatalytic hydrogen evolution over Cd0.5Zn0.5S by bismuth-doping. *Int. J. Hydrogen Energy* **2012**, *37*, 1366–1374. [CrossRef]
132. Wang, H.; Chen, W.; Zhang, J.; Huang, C.; Mao, L. Nickel nanoparticles modified CdS—A potential photocatalyst for hydrogen production through water splitting under visible light irradiation. *Int. J. Hydrogen Energy* **2015**, *40*, 340–345. [CrossRef]
133. Suzuki, T.; Hisatomi, T.; Teramura, K.; Shimodaira, Y.; Kobayashid, H.; Domen, K. A titanium-based oxysulfide photocatalyst: $La_5Ti_2MS_5O_7$ (M = Ag, Cu) for water reduction and oxidation. *Phys. Chem. Chem. Phys.* **2012**, *14*, 15475–15481. [CrossRef]
134. Kiyonori, O.; Akio, I.; Kentaro, T.; Kenji, T.; Michikazu, H.; Kazunari, D. Lanthanum–indium oxysulfide as a visible light driven photocatalyst for water splitting. *Chem. Lett.* **2007**, *36*, 854–855.
135. Zhang, L.; Han, Z.; Wang, W.; Li, X.; Su, Y.; Jiang, D.; Lei, X.; Sun, S. Solar-light-driven pure water splitting with ultrathin BiOCl nanosheets. *Chem. A Eur. J.* **2015**, *21*, 18089–18094. [CrossRef]

136. Han, Q.; Han, Q.; Wang, B.; Gao, J.; Cheng, Z.; Zhao, Y.; Zhang, Z.; Qu, L. Atomically thin mesoporous nanomesh of graphitic C_3N_4 for high-efficiency photocatalytic hydrogen evolution. *ACS Nano* **2016**, *10*, 2745–2751. [CrossRef] [PubMed]
137. Zheng, D.; Pang, C.; Wang, X. Teh function-led design of Z-scheme photocatalytic systems based on hollow carbon nitride semiconductors. *Chem. Commun.* **2015**, *51*, 17467–17470. [CrossRef] [PubMed]
138. Nayak, S.; Parida, K. Recent progress in LDH@graphene and analogous heterostructures for highly active and stable photocatalytic and photoelectrochemical water splitting. *Chem. Asian J.* **2021**, *16*, 2211–2248. [CrossRef] [PubMed]
139. Yang, Z.Z.; Zhang, C.; Zeng, G.M.; Tan, X.F.; Huang, D.L.; Zhou, J.W.; Fang, Q.Z.; Yang, K.H.; Wang, H.; Wei, J.; et al. State-of-the-art progress in the rational design of layered double hydroxide based photocatalysts for photocatalytic and photoelectrochemical H_2/O_2 production. *Coord. Chem. Rev.* **2021**, *446*, 214103. [CrossRef]
140. Zhang, J.; Zhang, W.; Yuan, F.; Yang, Z.; Lin, J.; Huang, Y.; Ding, M. Effect of Bi_5O_7I/calcined ZnAlBi-LDHs composites on Cr(VI) removal via adsorption and photocatalytic reduction. *Appl. Surf. Sci.* **2021**, *562*, 150129. [CrossRef]
141. Gao, R.; Yan, D. Recent development of Ni/Fe-based micro/nanostructures toward photo/electrochemical water oxidation. *Adv. Energy Mater.* **2020**, *10*, 1900954. [CrossRef]
142. Zhao, D.; Jiang, K.; Pi, Y.; Huang, X. Superior electrochemical oxygen evolution enabled by three-dimensional layered double hydroxide nanosheet superstructures. *ChemCatChem* **2017**, *9*, 84–88. [CrossRef]